nature immunology

ARTICLES

https://doi.org/10.1038/s41590-019-0480-4

PTPN2 regulates the generation of exhausted CD8+ T cell subpopulations and restrains tumor immunity

Martin W. LaFleur[1,2,3,4], Thao H. Nguyen[1,3], Matthew A. Coxe[1,3], Brian C. Miller[1,2,3,5,6], Kathleen B. Yates[2,5], Jacob E. Gillis[1,3], Debattama R. Sen[2,4,5], Emily F. Gaudiano[1,3], Rose Al Abosy[2], Gordon J. Freeman[6], W. Nicholas Haining[2,5,7*] and Arlene H. Sharpe[1,3,5,7*]

CD8+ T cell exhaustion is a state of dysfunction acquired in chronic viral infection and cancer, characterized by the formation of Slamf6+ progenitor exhausted and Tim-3+ terminally exhausted subpopulations through unknown mechanisms. Here we establish the phosphatase PTPN2 as a new regulator of the differentiation of the terminally exhausted subpopulation that functions by attenuating type 1 interferon signaling. Deletion of *Ptpn2* in CD8+ T cells increased the generation, proliferative capacity and cytotoxicity of Tim-3+ cells without altering Slamf6+ numbers during lymphocytic choriomeningitis virus clone 13 infection. Likewise, *Ptpn2* deletion in CD8+ T cells enhanced Tim-3+ anti-tumor responses and improved tumor control. Deletion of *Ptpn2* throughout the immune system resulted in MC38 tumor clearance and improved programmed cell death-1 checkpoint blockade responses to B16 tumors. Our results indicate that increasing the number of cytotoxic Tim-3+CD8+ T cells can promote effective anti-tumor immunity and implicate PTPN2 in immune cells as an attractive cancer immunotherapy target.

T cell exhaustion is a state of dysfunction observed in CD8+ T cells during chronic viral infection and cancer[1–4]. During chronic viral infections, exhausted CD8+ T cells progressively lose functional capabilities, such as cytokine production, cytotoxicity and proliferative capacity[5,6]. During the progression to exhaustion, T cells have reduced functional capacity compared to effector CD8+ T cells[7], yet still have the potential to form memory cells if removed from chronic antigen stimulation[8]. The program of exhaustion[9–11] is initiated during chronic antigen stimulation[12,13] and likely evolved as a mechanism to prevent excessive immunopathology during chronic antigenic insults[14].

There are two subpopulations of exhausted CD8+ T cells, each with distinct functional properties. The progenitor population of exhausted cells, defined as programmed cell death (PD)-1^{int} (ref. [15]), CXCR5+ (refs. [16,17]) or Slamf6+ (ref. [4]), possesses enhanced proliferative capacity and polyfunctional cytokine production and serves as a reservoir of cells for the terminally exhausted population. The terminally exhausted population is defined as PD-1^{hi} (ref. [15]) or Tim-3+(refs. [16,17]) and is cytotoxic, albeit having reduced proliferative capacity, longevity and polyfunctional cytokine production. *Eomes*, *Id2*, *Runx3*, T cell receptor (TCR) stimulation, interleukin (IL)-2, IL-21, IL-12 and type 1 interferon (IFN)-I promote the formation of the terminally exhausted subpopulation[15,16,18–21], whereas *Tbet*, *Tcf7* and *Bcl6* enhance the formation of the progenitor exhausted subpopulation[15,17,18]. During responses to PD-1 immune checkpoint blockade (ICB), the progenitor population expands and gives rise to the terminally exhausted subset[17]. These subsets are found in murine and human tumors[4,18,22–27], and an increased ratio of progenitor to terminally exhausted cells is correlated with responsiveness to ICB in melanoma patients[24]. Given their distinct functions and responses to anti-PD-1, there is an urgent need to identify therapeutic targets that regulate the balance and functionality of exhausted subpopulations in cancer.

Here we identify PTPN2 as a regulator of the generation of the Tim-3+ subpopulation. *Ptpn2* deletion is associated with enhanced IFN-α cytokine signaling and increased the number of Tim-3+ cytotoxic CD8+ T cells during lymphocytic choriomeningitis virus (LCMV) clone 13 infection without altering Slamf6+ cell numbers. Furthermore, *Ptpn2* deletion promotes formation of the Tim-3+ subset and increases Tim-3+CD8+ T cell responses in MC38 and B16 cancer models. This leads to complete clearance of MC38 tumors and improved PD-1 ICB responses to B16 tumors. Our data demonstrate that increasing the number of Tim-3+ cytotoxic CD8+ T cells can promote effective tumor immunity and provides a rationale for PTPN2 as a cancer immunotherapy target.

Results

Loss of *Ptpn2* promotes the early proliferation of CD8+ T cells during LCMV clone 13 infection. We recently conducted a pooled in vivo loss-of-function screen and identified PTPN2 as a candidate regulator of CD8+ T cell responses[28]. To examine the role of PTPN2 in LCMV clone 13 infection, we created bone marrow chimeras using CHIME (CHimeric IMmune Editing), a chimera-based CRISPR-Cas9 delivery method (Fig. 1a)[28] to delete *Ptpn2* in hematopoietic cells from P14 TCR transgenic mice (specific for the LCMV CD8 epitope, $GP_{33–41}$). We confirmed the efficient deletion (~80%) of *Ptpn2* in naive P14 CD8+ T cells using the tracking of indels by decomposition (TIDE) assay[29] (Fig. 1b). To evaluate cell-intrinsic functions of PTPN2 in CD8+ T cells, we cotransferred congenically marked naive P14 TCR transgenic *Ptpn2* single guide (sg) RNA-containing (*Ptpn2*-deleted) and control sgRNA-containing (control) CD8+ T cells to wild-type recipient mice and subsequently

[1]Department of Immunology, Blavatnik Institute, Harvard Medical School, Boston, MA, USA. [2]Department of Pediatric Oncology, Dana-Farber Cancer Institute, Boston, MA, USA. [3]Evergrande Center for Immunological Diseases, Harvard Medical School and Brigham and Women's Hospital, Boston, MA, USA. [4]Division of Medical Sciences, Harvard Medical School, Boston, MA, USA. [5]Broad Institute of Harvard and Massachusetts Institute of Technology, Cambridge, MA, USA. [6]Department of Medical Oncology, Dana-Farber Cancer Institute, Boston, MA, USA. [7]These authors contributed equally: W. Nicholas Haining, Arlene H. Sharpe. *e-mail: nick.haining@merck.com; Arlene_Sharpe@hms.harvard.edu

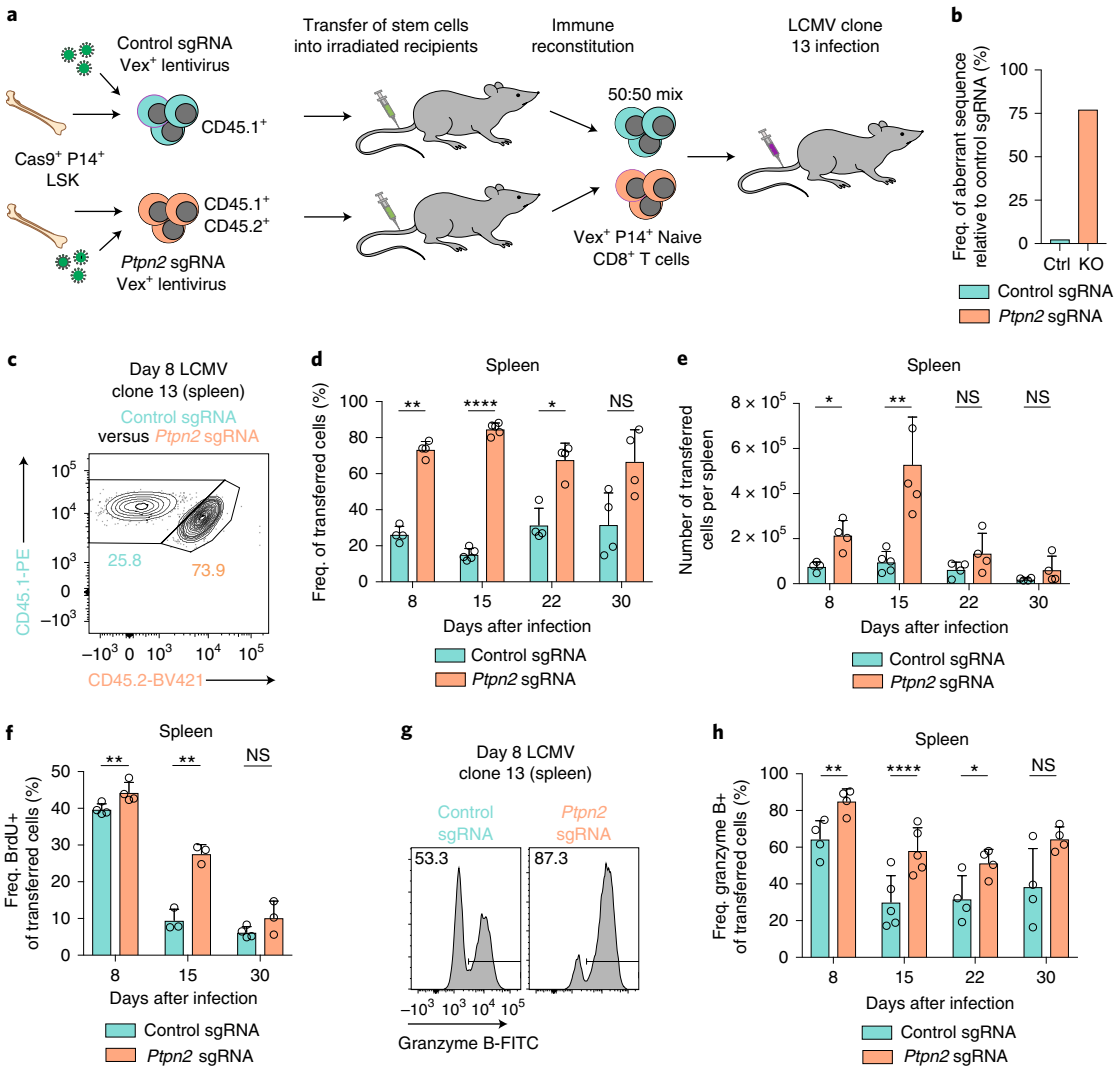

Fig. 1 | Loss of *Ptpn2* promotes the early proliferation of CD8⁺ T cells during LCMV clone 13 infection. a, Schematic of cotransfer experiment during LCMV clone 13 infections. Chimeric mice were generated using the CHIME system. LSK, lineage⁻ Sca-1⁺ c-Kit⁺. **b**, TIDE assay on naive CD8⁺ T cells for a control (ctrl) and *Ptpn2*-targeting sgRNA. Data are representative of four independent experiments, $n = 1$ mouse. KO, knockout. **c**, Representative flow cytometry plot of cotransferred control or *Ptpn2*-deleted P14 T cells in the spleen 8 d after LCMV clone 13 infection. Data are representative of eight independent experiments, $n \geq 4$ mice. **d**,**e**, Frequency (freq.) of CD45.1⁺ transferred cells (**d**) and number of control or *Ptpn2*-deleted P14 T cells (**e**) in the spleen 8, 15, 22 and 30 d after LCMV clone 13 infection. Representative of two independent experiments, $n \geq 4$ mice. **f**, Quantification of BrdU incorporation for cotransferred control and *Ptpn2*-deleted P14 T cells 8, 15 and 30 d after LCMV clone 13 infection. Data are representative of two independent experiments, $n \geq 3$ mice. **g**, Representative flow cytometry plots of granzyme B expression from splenic control or *Ptpn2*-deleted P14 CD8⁺ T cells cotransferred at 8 d after LCMV clone 13 infection as in (**c**). Data are representative of two independent experiments, $n \geq 4$ mice. **h**, Quantification of **g**, 8, 15, 22 and 30 d after LCMV clone 13 infection. Data are representative of two independent experiments, $n \geq 4$ mice. Bar graphs represent the mean and error bars represent s.d. Statistical significance was assessed by a two-sided Student's paired *t*-test (**d**–**f**,**h**) (not significant (NS), $P > 0.05$, $^{*}P \leq 0.05$, $^{**}P \leq 0.01$, $^{***}P \leq 0.001$, $^{****}P \leq 0.0001$). See also Supplementary Fig. 1. Panel **a** adapted from ref. [28], Springer Nature Ltd.

infected them with LCMV clone 13. Given that *Ptpn2* deficiency leads to alterations in thymocyte maturation and aberrant T cell activation at homeostasis[30], we transferred only naive CD44⁻ CD62L⁺ cells before LCMV infection (Supplementary Fig. 1a). These cells did not express effector-related molecules, such as granzyme B (Supplementary Fig. 1b) or markers of cell proliferation, such as Ki-67 or 5-bromodeoxyuridine (BrdU) incorporation (Supplementary Fig. 1c,d). Following LCMV infection, there was a significant increase in the *Ptpn2*-deleted cells compared to control cells at 8 d and 15 d after infection, but not 30 d after infection (Fig. 1c–e and Supplementary Fig. 1e). The increased cell numbers at these time points were due, in part, to increased proliferation of *Ptpn2*-deleted cells (Fig. 1f). Deletion of *Ptpn2* also increased the percentage of granzyme B⁺ cells at early time points (Fig. 1g,h) but did not affect the percentage of IFN-γ⁺ TNF⁺ cells (Supplementary Fig. 1f). Thus, *Ptpn2* deletion provides CD8⁺ T cells with a transient advantage early during LCMV clone 13 infection but does not prevent contraction at later time points.

Deletion of *Ptpn2* enhances formation of the Tim-3⁺ terminally exhausted subpopulation during LCMV clone 13 infection. The changes in granzyme B expression prompted us to examine the impact of *Ptpn2* deletion on the generation of the Slamf6⁺ and Tim-3⁺ subpopulations. *Ptpn2* deletion increased the ratio of Tim-3⁺ to Slamf6⁺ cells at 8, 15 and 22 d after infection (Fig. 2a,b), despite transferring only Slamf6⁺Tim-3⁻ cells (Supplementary Fig. 2a).

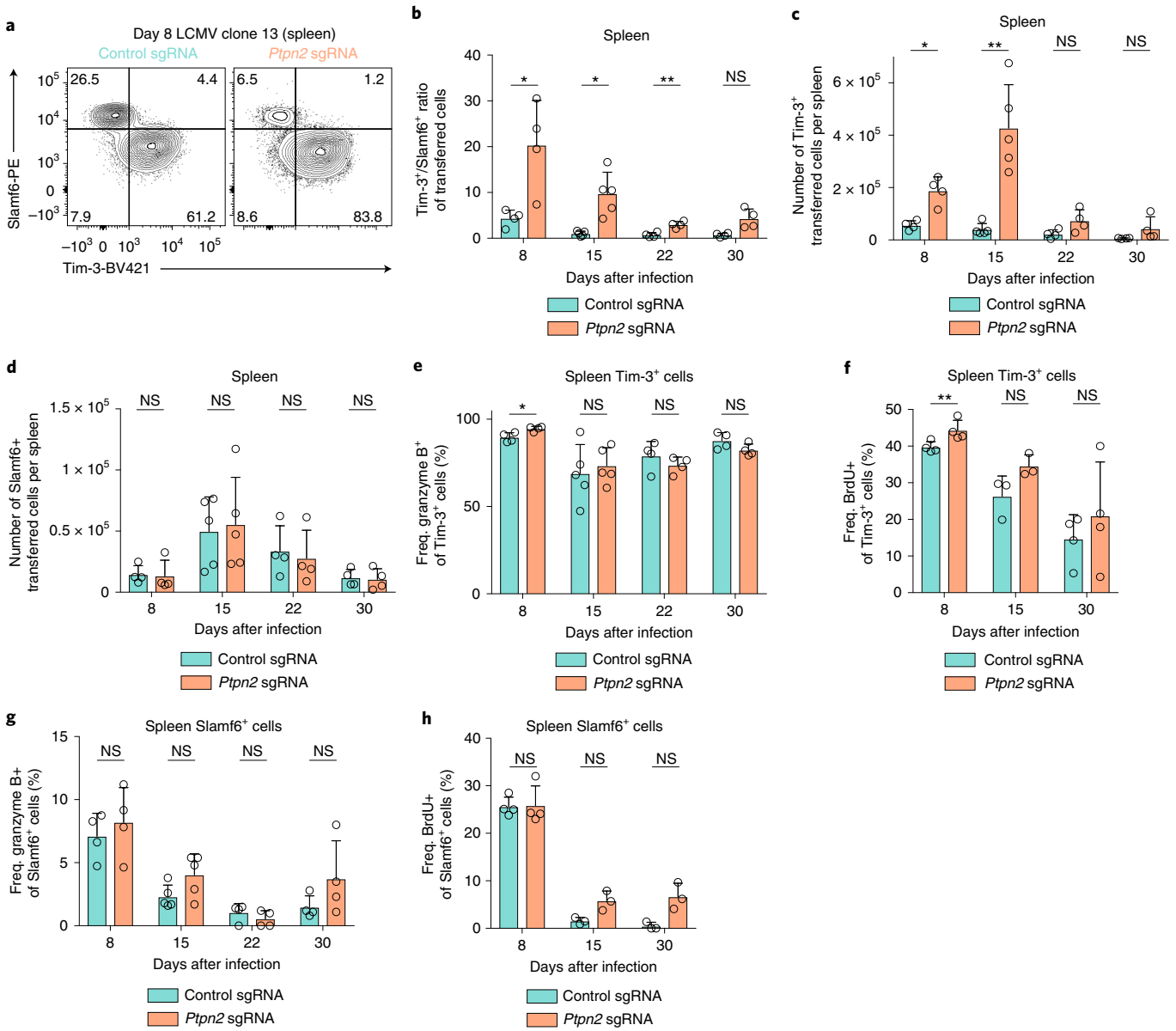

Fig. 2 | Deletion of *Ptpn2* enhances formation of the Tim-3$^+$ terminally exhausted subpopulation during LCMV Clone 13 infection. a, Representative flow cytometry plots of Tim-3 and Slamf6 expression on control or *Ptpn2*-deleted P14 T cells in the spleen 8 d after LCMV clone 13 infection. Data are representative of eight independent experiments, $n \geq 4$ mice. **b**, Ratio of Tim-3$^+$/Slamf6$^+$ control or *Ptpn2*-deleted P14 T cells in the spleen 8, 15, 22 and 30 d after LCMV clone 13 infection. Data are representative of two independent experiments, $n \geq 4$ mice. **c**, Number of Tim-3$^+$ control or *Ptpn2*-deleted P14 T cells in the spleen 8, 15, 22 and 30 d after LCMV clone 13 infection. Data are representative of two independent experiments, $n \geq 4$ mice. **d**, Number of Slamf6$^+$ control or *Ptpn2*-deleted P14 T cells in the spleen 8, 15, 22 and 30 d after LCMV clone 13 infection. Data are representative of two independent experiments, $n \geq 4$ mice. **e**, Quantification of granzyme B expression for Tim-3$^+$ control or *Ptpn2*-deleted P14 T cells in the spleen 8, 15, 22 and 30 d after LCMV clone 13 infection. Data are representative of two independent experiments, $n \geq 4$ mice. **f**, Quantification of BrdU incorporation for Tim-3$^+$ control or *Ptpn2*-deleted P14 T cells in the spleen 8, 15 and 30 d after LCMV clone 13 infection. Data are representative of two independent experiments, $n \geq 3$ mice. **g**, Quantification of granzyme B expression for Slamf6$^+$ control or *Ptpn2*-deleted P14 T cells in the spleen 8, 15, 22 and 30 d after LCMV clone 13 infection. Data are representative of two independent experiments, $n \geq 4$ mice. **h**, Quantification of BrdU incorporation for Slamf6$^+$ control or *Ptpn2*-deleted P14 T cells in the spleen 8, 15 and 30 d after LCMV clone 13 infection. Data are representative of two independent experiments, $n \geq 3$ mice. Bar graphs represent the mean and error bars represent the s.d. Statistical significance was assessed by a two-sided Student's paired *t*-test (**b**–**h**) (NS, $P > 0.05$, $^*P \leq 0.05$, $^{**}P \leq 0.01$, $^{***}P \leq 0.001$, $^{****}P \leq 0.0001$). See also Supplementary Fig. 2.

Analysis of the populations using Tim-3 and a distinct progenitor marker (CXCR5) (refs. [4,16,17]) gave identical results (Supplementary Fig. 2b,c). Moreover, following *Ptpn2* deletion, we observed a significant reduction in expression of two additional markers of progenitor exhausted cells, CD127 and TCF1 (Supplementary Fig. 2d). The increase in the Tim-3$^+$ to Slamf6$^+$ ratio was driven by a specific increase in the number of Tim-3$^+$ cells following *Ptpn2* deletion (Fig. 2c), whereas there was no difference in the number of Slamf6$^+$ cells (Fig. 2d), nor CXCR5$^+$ cells (Supplementary Fig. 2e). Furthermore, in non-TCR transgenic chimeras, *Ptpn2* deletion resulted in an increase in the percentage of Tim-3$^+$ cells and a decrease in the percentage of Slamf6$^+$ cells compared to control cells

(Supplementary Fig. 2f). Thus, deletion of *Ptpn2* enhances formation of the Tim-3$^+$ subset during LCMV clone 13 infection.

To determine whether changes in granzyme B expression and BrdU incorporation (Fig. 1f–h) were intrinsically changed in the Tim-3$^+$ subpopulations, we compared cotransferred control and *Ptpn2*-deleted cells and found only a minimal increase in granzyme B expression in the *Ptpn2*-deleted Tim-3$^+$ cells (Fig. 2e). In addition, we found a nominal increase in BrdU incorporation between control and *Ptpn2*-deleted Tim-3$^+$ cells (Fig. 2f), indicating a similar increase in actively proliferating cells. We found no differences in granzyme B expression nor BrdU incorporation in Slamf6$^+$ control and *Ptpn2*-deleted cells (Fig. 2g,h). These findings demonstrate that *Ptpn2* deletion leads to a specific increase in the generation of the Tim-3$^+$ subpopulation, while preserving the number of Slamf6$^+$ cells, and that the altered ratio of Tim-3$^+$ to Slamf6$^+$ cells is primarily responsible for the observed increase in granzyme B expression and BrdU incorporation.

***Ptpn2* deletion promotes effector-skewed Slamf6$^+$ and Tim-3$^+$ subpopulations during LCMV infection.** We next performed single-cell RNA-sequencing (RNA-seq) on control and *Ptpn2*-deleted cells 30 d after LCMV infection, because the canonical features of exhaustion are present at this time point[5,10]. Unsupervised clustering of the cells revealed six subpopulations, which we identified by marker gene expression and previously defined signature enrichment (Fig. 3a,b and Supplementary Fig. 3a,b). We recapitulated the previously described terminally exhausted, progenitor exhausted, proliferating and effector-like populations[4], and identified a distinct IFN-responsive cluster that contained both progenitor exhausted and terminally exhausted cells, suggesting that the cluster represented cells that were actively responding to IFN-α (Fig. 3b and Supplementary Fig. 3b). Further analysis of the distribution of the control or *Ptpn2*-deleted cells across the clusters revealed a significant skewing of the control cells into the progenitor exhausted cluster and the *Ptpn2*-deleted cells into the effector-like, proliferating and terminally exhausted clusters (Fig. 3c,d), consistent with our flow cytometry data (Supplementary Fig. 3c). We also noted that within a subpopulation, the *Ptpn2*-deleted cells or control CD8$^+$ T cells tended to cluster together (Supplementary Fig. 3d). Differential expression analysis between *Ptpn2*-deleted and control cells within the progenitor and terminally exhausted clusters revealed that the *Ptpn2*-deleted cells had increased expression of genes associated with terminally exhausted or effector cells such as *Gzma*, *Cd160*, *Ccl4* and *Ccl5* (adjusted *P* values <0.005), consistent with an enrichment of effector-related gene signatures (Fig. 3e,f). Thus, at 30 d after LCMV infection, *Ptpn2*-deleted progenitor and terminally exhausted cells have increased transcription of effector-related genes.

We next asked whether *Ptpn2* deletion impacted the cell states of Slamf6$^+$ and Tim-3$^+$ subpopulations at an earlier time point after LCMV infection. We performed RNA-seq on cotransferred *Ptpn2*-deleted or control CD8$^+$ T cells 8 d after LCMV clone 13 infection (Supplementary Table 1) and found that the Slamf6$^+$ and Tim-3$^+$ subpopulations clustered together regardless of *Ptpn2* deletion (Supplementary Fig. 3e). Gene set enrichment analysis (GSEA) revealed that both control and *Ptpn2*-deleted Slamf6$^+$ cells were significantly enriched for the LCMV Slamf6 versus Tim-3 Up signature[4], whereas the control and *Ptpn2*-deleted Tim-3$^+$ cells were significantly enriched for the LCMV Slamf6 versus Tim-3 Down signature[4] (Supplementary Fig. 3f). Consistent with this, *Ptpn2* deletion had almost no effect on the epigenetic state of either the Slamf6$^+$ or Tim-3$^+$ populations (<0.25% of open chromatin regions differentially expressed) 8 d after infection (Supplementary Fig. 3g and Supplementary Table 2). Both control and *Ptpn2*-deleted CD8$^+$ T cells still showed characteristic differences between the Slamf6$^+$ and Tim-3$^+$ populations (Supplementary Fig. 3h). In addition, both control and *Ptpn2*-deleted cells showed chromatin-accessible regions at the *Tox* locus (Supplementary Fig. 3i), characteristic of T cell exhaustion[10], indicating the cells were differentiating into the exhausted subpopulations.

Although the general states of the Slamf6$^+$ and Tim-3$^+$ cells were maintained at day 8, GSEA of the Slamf6$^+$ and Tim-3$^+$ *Ptpn2*-deleted cells compared to control cells revealed an enrichment for effector-related gene signatures (Fig. 3g,h). Within both the Slamf6$^+$ and Tim-3$^+$ subpopulations, *Ptpn2*-deleted cells had increased expression of effector-related genes pertaining to cytotoxicity (*Gzmk*, *Lamp2*, *Serpina3g*) and proliferation (*Stmn1*, *Tk1*, *Tpi1*), compared to control cells (Fig. 3i,j). Thus, while *Ptpn2* deletion does not fundamentally change the Slamf6$^+$ and Tim-3$^+$ subpopulations, it does lead to increases in Tim-3$^+$ cell numbers and robustly increases effector-related genes both early and late after LCMV infection.

Consistent with the increase in effector-like profiles in the *Ptpn2*-deleted cells, *Ptpn2*-deleted CD8$^+$ T cells had increased cytotoxic potential (Fig. 3k). This increased killing potential was due to an intrinsic change within the Tim-3$^+$ cells, as *Ptpn2*-deleted Tim-3$^+$ cells showed increased killing of target cells when compared with control cells (Fig. 3l). Overall, these findings validate the observed enrichment in cytotoxic genes seen by RNA-seq and demonstrate that *Ptpn2* deletion improves the cytotoxic function of CD8$^+$ T cells.

***Ptpn2* deletion increases Tim-3$^+$ cell differentiation and proliferation.** The increase in Tim-3$^+$ cell numbers at 8 d after LCMV

Fig. 3 | *Ptpn2* deletion promotes effector-skewed Slamf6$^+$ and Tim-3$^+$ subpopulations during LCMV infection. a, A t-distributed stochastic neighbor embedding (tSNE) projection of single-cell RNA-seq profiles from 7,027 control or *Ptpn2*-deleted P14$^+$ CD8$^+$ T cells 30 d after LCMV clone 13 infection. Clusters are distinct colors. Data are representative of one experiment, $n = 4$ pooled mice. APC, antigen-presenting cell. **b**, Enrichment of gene signatures in the clusters. Data are representative of one experiment, $n = 4$ pooled mice. **c**, Plots depicting the intercluster density for control or *Ptpn2*-deleted cells. Data are representative of one experiment, $n = 4$ pooled mice. **d**, Quantification of the proportion of control or *Ptpn2*-deleted cells in each cluster. Error bars represent the 95% CI and the dotted line represents the proportion of *Ptpn2*-deleted cells among all cells projected. Data are representative of one experiment, $n = 4$ pooled mice. **e**,**f**, Signature enrichments of cotransferred control and *Ptpn2*-deleted cells from the progenitor (**e**) or terminally exhausted clusters (**f**). Eff, effector. Mem, memory. Data are representative of one experiment, $n = 4$ pooled mice. **g**,**h**, GSEA curves for significantly enriched signatures in Slamf6$^+$ cells (**g**) and Tim-3$^+$ cells (**h**) for bulk RNA-seq of cotransferred control and *Ptpn2*-deleted cells 8 d after LCMV clone 13 infection. Data are representative of one experiment, $n = 2$ mice with $n = 2$ technical replicates per mouse. FDR, false discovery rate. T-conv, T cells in conventional lineage. **i**,**j**, Row-normalized heat map of effector-associated genes in Slamf6$^+$ cells (**i**) and Tim-3$^+$ cells (**j**) for bulk RNA-seq of cotransferred control and *Ptpn2*-deleted cells 8 d after LCMV clone 13 infection. Data are representative of one experiment, $n = 2$ mice with $n = 2$ technical replicates per mouse. **k**, Quantification of frequency of tumor cells killed when cocultured with control or *Ptpn2*-deleted CD8$^+$ T cells (2:1 effector:target ratio) isolated from 8 d LCMV clone 13 infection. Data are representative of two independent experiments, $n = 5$ mice. **l**, Quantification of frequency of tumor cells killed when cocultured with Tim-3$^+$ control or Tim-3$^+$ *Ptpn2*-deleted CD8$^+$ T cells (2:1 effector:target ratio) isolated from 8 d LCMV clone 13 infection. Data are representative of two independent experiments, $n = 5$ mice. Statistical significance was assessed by the two-sided Wilcoxon rank sum test (**b**,**e**,**f**), two-sided binomial test (**d**), two-sided Kolmogorov–Smirnov test (**g**–**h**) and two-sided Student's paired *t*-test (**k**–**l**) (NS, $P > 0.05$, $^*P \leq 0.05$, $^{**}P \leq 0.01$, $^{***}P \leq 0.001$, $^{****}P \leq .00001$). See also Supplementary Fig. 3.

infection, coupled with the enhanced effector-related gene signatures, led us to ask whether PTPN2 was impacting the differentiation of these subpopulations. We found that *Ptpn2*-deleted CD8$^+$ T cells had a marked competitive advantage over control cells 4 d after infection (Fig. 4a) and enhanced differentiation into Tim-3$^+$ cells (Fig. 4b). *Ptpn2* deletion resulted in a decreased percentage of Slamf6$^+$Tim-3$^-$ cells and an increased percentage of Slamf6$^+$Tim-3$^+$ cells and Slamf6$^-$Tim-3$^+$ cells (Fig. 4c), as well as an increase in granzyme B expression (Fig. 4d). We then asked whether the increase in the number and percentage of Tim-3$^+$ cells was owing to (1) increased conversion from Slamf6$^+$ cells[4,16,17]; (2) increased proliferative capacity of either population; or (3) increased persistence (Fig. 4e). First, to test conversion, we isolated antigen-experienced control or *Ptpn2*-deleted Slamf6$^+$ cells (Fig. 4e) and restimulated them in vitro with signals 1–3 (anti-CD3, anti-CD28 and IFN-α together)[31], as well as IL-2, and found that *Ptpn2*-deleted Slamf6$^+$ cells preferentially formed Slamf6$^+$Tim-3$^+$ and Slamf6$^-$Tim-3$^+$ subsets compared to control cells (Fig. 4f). Second, we tested

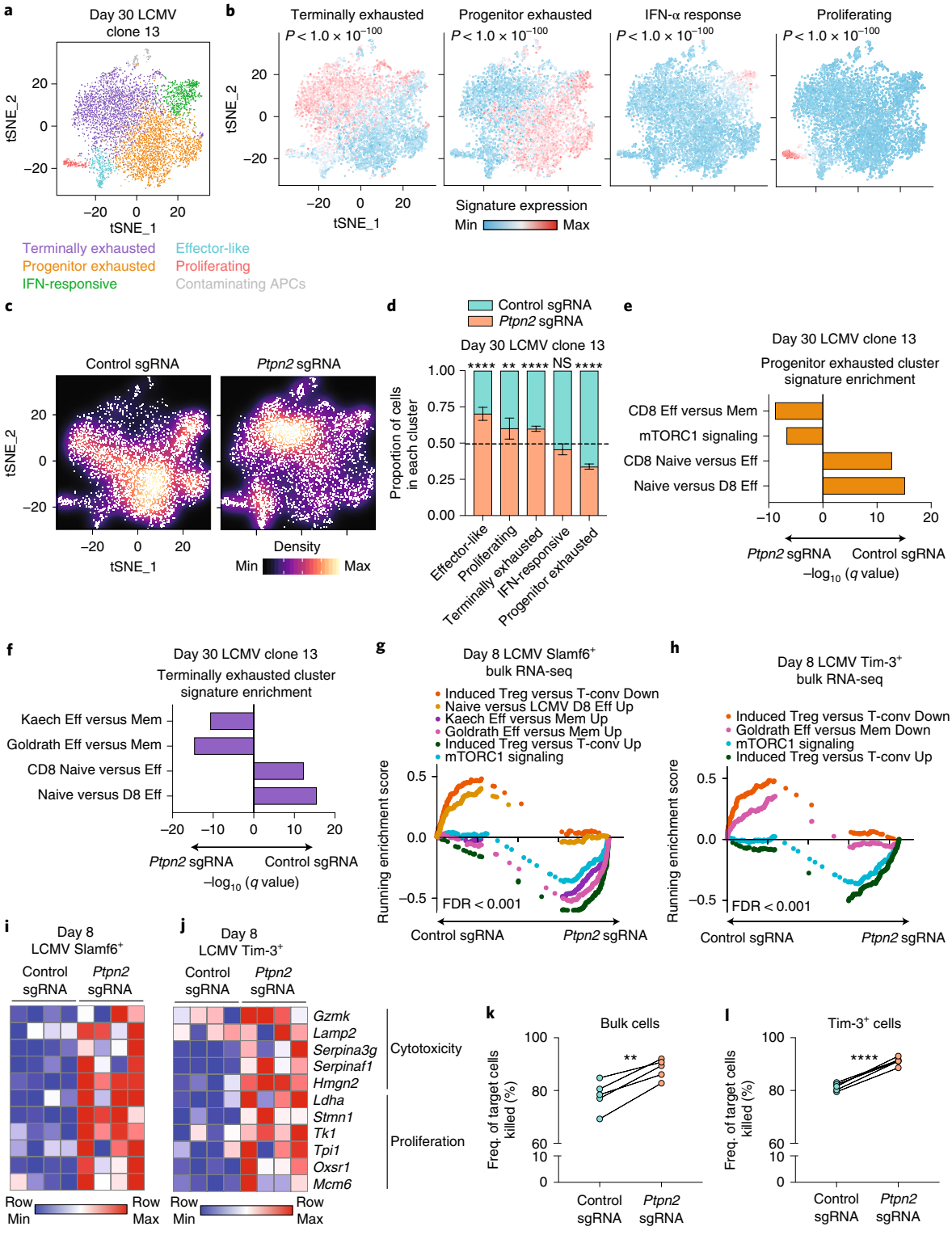

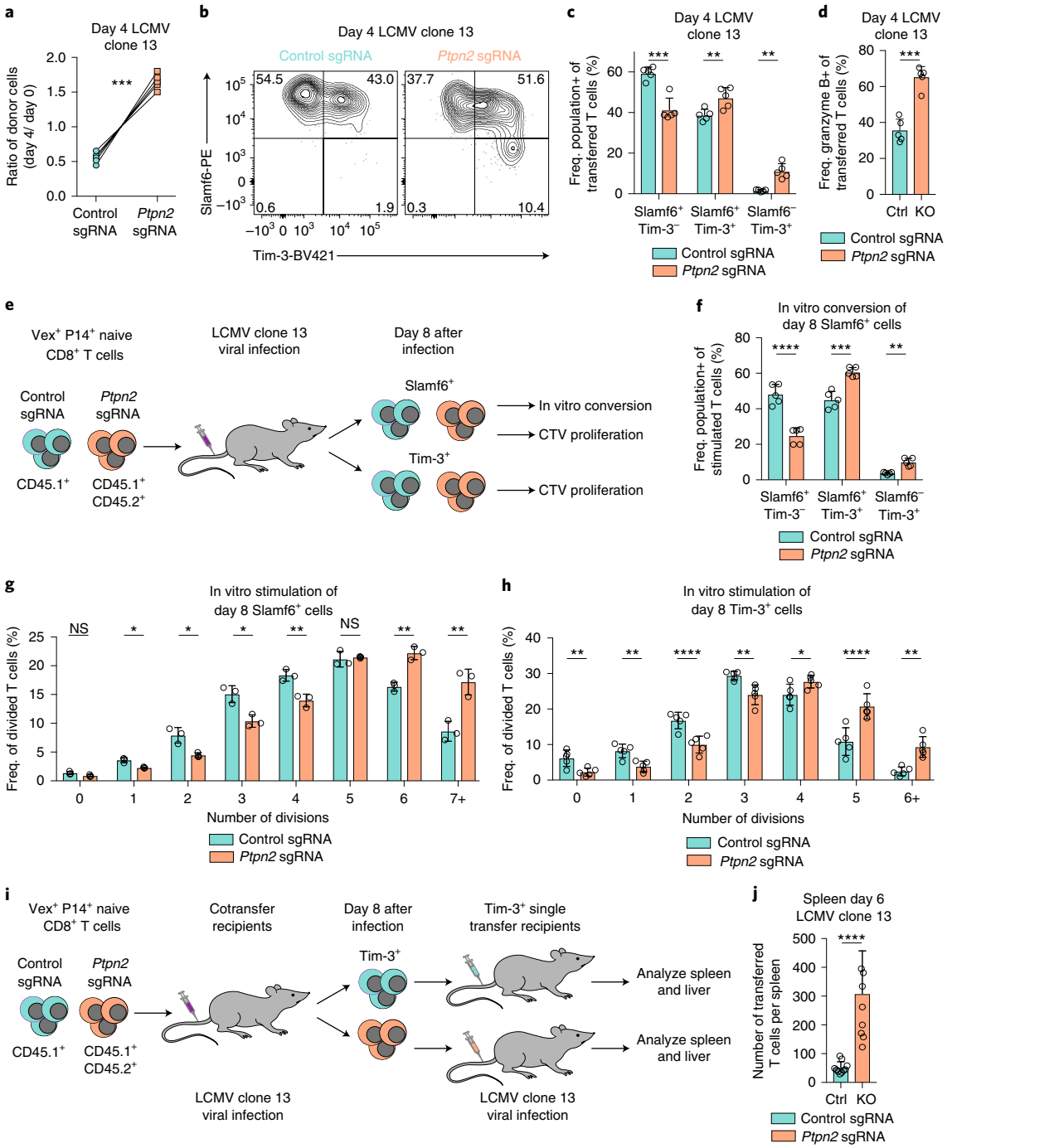

Fig. 4 | *Ptpn2* deletion increases Tim-3$^+$ cell differentiation and proliferation. a, Quantification of frequencies of cotransferred control or *Ptpn2*-deleted CD8$^+$ T cells 4 d after LCMV clone 13 infection. Frequencies at day 4 were normalized to input frequencies at day 0. Data are representative of two independent experiments, $n=5$ mice. **b**, Representative flow cytometry plots of Slamf6 and Tim-3 expression on splenic CD8$^+$ T cells 4 d after LCMV clone 13 infection for cotransferred control and *Ptpn2*-deleted cells. Data are representative of two independent experiments, $n=5$ mice. **c**, Quantification of Slamf6$^+$Tim-3$^-$, Slamf6$^+$Tim-3$^+$ and Slamf6$^-$Tim-3$^+$ subsets in **b**. Data are representative of two independent experiments, $n=5$ mice. **d**, Quantification of granzyme B expression of cells as in **a**. Data are representative of two independent experiments, $n=5$ mice. **e**, Schematic of in vitro conversion and CTV proliferation assays using cotransferred control or *Ptpn2*-deleted CD8$^+$ T cells isolated at 8 d after LCMV clone 13 infection. **f**, Quantification of Slamf6$^+$Tim-3$^-$, Slamf6$^+$Tim-3$^+$ and Slamf6$^-$Tim-3$^+$ subsets following in vitro stimulation (anti-CD3/CD28 with IL-2 and IFN-α) of control or *Ptpn2*-deleted CD8$^+$ T cells isolated at 8 d after LCMV clone 13 infection. Data are representative of two independent experiments, $n=5$ mice. **g**,**h**, Quantification of frequency of divisions following in vitro stimulation (anti-CD3/CD28 with IL-2) of CTV-labeled Slamf6$^+$ (**g**) or CTV-labeled Tim-3$^+$ (**h**), control or *Ptpn2*-deleted CD8$^+$ T cells isolated at 8 d after LCMV clone 13 infection. Data are representative of two independent experiments, $n=3$ mice (**g**), $n=5$ mice (**h**). **i**, Schematic of in vivo persistence assay of Tim-3$^+$ cells. **j**, Quantification of number of recovered Tim-3$^+$ control or *Ptpn2*-deleted cells in the spleen 6 d after LCMV clone 13 infection, following the transfer of these cells which were previously isolated at 8 d after LCMV clone 13 infection. Data are representative of two pooled experiments, $n=8$ mice. Bar graphs represent the mean and error bars represent the s.d. Statistical significance was assessed by two-sided Student's paired *t*-test (**a**,**c**,**d**,**f**–**h**) or two-sided Student's unpaired *t*-test (**j**) (NS, $P>0.05$, $^*P\leq0.05$, $^{**}P\leq0.01$, $^{***}P\leq0.001$, $^{****}P\leq0.0001$). See also Supplementary Fig. 4. Panels **e**,**i** adapted from ref. [28], Springer Nature Ltd.

proliferative capacity following restimulation and found that antigen-experienced *Ptpn2*-deleted Slamf6$^+$ cells underwent more rounds of division than control Slamf6$^+$ cells (Fig. 4g and Supplementary Fig. 4a,b). When BrdU incorporation was assessed previously, there was comparable incorporation between control and *Ptpn2*-deleted Slamf6$^+$ cells, indicating similar active proliferation (Fig. 2h). Here, the increase in CellTrace Violet (CTV) dilution signifies enhanced proliferative capacity of the *Ptpn2*-deleted Slamf6$^+$ cells compared to control cells. We also compared the proliferative capacity of antigen-experienced control and *Ptpn2*-deleted Tim-3$^+$ cells following restimulation and found that *Ptpn2*-deleted Tim-3$^+$ cells also underwent more rounds of division than control Tim-3$^+$ cells (Fig. 4h and Supplementary Fig. 4c,d). Thus, while the *Ptpn2*-deleted Slamf6$^+$ and Tim-3$^+$ cells have a similar frequency of actively proliferating cells compared to control cells (Fig. 2f,h), they had the greatest difference in proliferative capacity (Fig. 4g,h).

To examine the persistence of Tim-3$^+$ cells in vivo, we transferred antigen-experienced control or *Ptpn2*-deleted Tim-3$^+$ cells separately to new recipients infected with LCMV clone 13 (Fig. 4i). We recovered an increased number of *Ptpn2*-deleted Tim-3$^+$ cells compared to control cells in the spleen and liver (Fig. 4j and Supplementary Fig. 4e). We also found a decrease in survival of the recovered *Ptpn2*-deleted Tim-3$^+$ cells (Supplementary Fig. 4f), suggesting that their increased cell number was likely owing to a proliferative advantage (Fig. 4h), consistent with the known role of PTPN2 in regulating the proliferative capacity of naive CD8$^+$ T cells by dephosphorylation of kinases downstream of the TCR[30]. Thus, these findings demonstrate that *Ptpn2* deletion affects the generation of Tim-3$^+$ cells in multiple ways: by enhancing conversion of Slamf6$^+$ cells into Tim-3$^+$ cells and increasing the proliferative capacities of both Slamf6$^+$ and Tim-3$^+$ cells.

***Ptpn2* deletion increases Tim-3$^+$ cell differentiation through enhanced IFN-α signaling.** We next determined the factors driving the increased differentiation of Slamf6$^+$ cells into Tim-3$^+$ cells following *Ptpn2* deletion. We evaluated the necessity of IL-2 and IFN-α, as these cytokines have important roles in the differentiation of the Tim-3$^+$ subpopulation during LCMV clone 13 infection[18,20] and lead to phosphorylation of STAT5 and STAT1, respectively, both known targets of PTPN2 (refs. [32,33]). We stimulated control or *Ptpn2*-deleted naive CD8$^+$ T cells with anti-CD3/CD28 plus IL-2, IFN-α, both IL-2 and IFN-α, or blocking antibodies to abolish IL-2 and IFN-α signaling. Stimulation with IL-2, IFN-α and IL-2 plus IFN-α led to increased CD25 expression on *Ptpn2*-deleted cells compared to control cells (Supplementary Fig. 5a), indicating increased activation[30]. Consistent with antigen-experienced Slamf6$^+$ cells, stimulation of naive Slamf6$^+$ cells with IL-2 plus IFN-α resulted in a decreased percentage of Slamf6$^+$Tim-3$^-$ cells and an increased percentage of Slamf6$^+$Tim-3$^+$ and Slamf6$^-$Tim-3$^+$ cells in the *Ptpn2*-deleted cells, compared to control cells (Figs. 5a–c and Supplementary Fig. 5b). However, the addition of IL-2 or IFN-α separately was unable to recapitulate the marked increase of Slamf6$^-$Tim-3$^+$ cells observed following treatment with the combination (Fig. 5c). Moreover, CD28 costimulation was also required for the differentiation of Slamf6$^-$Tim-3$^+$ cells (Supplementary Fig. 5c). We also ruled out the contribution of soluble factors, as conditioned supernatant from *Ptpn2*-deleted cells did not increase the percentage of Slamf6$^-$Tim-3$^+$ cells compared to control cells (Supplementary Fig. 5d). Thus, IL-2, IFN-α and CD28 were all required for the enhanced generation of Tim-3$^+$ cells in *Ptpn2*-deleted CD8$^+$ T cells in our in vitro stimulation assay.

Given the requirement for IFN-α in vitro and the known role for IFN-I signaling in the regulation of Tim-3$^+$ and Slamf6$^+$ subpopulations[18], we next investigated the impact of *Ptpn2* deletion on STAT1 phosphorylation. *Ptpn2*-deleted cells had an increased percentage and duration of pSTAT1 expression (Fig. 5d), despite comparable levels of the type 1 interferon receptor (IFNAR1) (Supplementary Fig. 5e). This increase in pSTAT1 was observed in both Slamf6$^+$ and Tim-3$^+$ subsets (Fig. 5e,f). Consistent with this, IFN-I signaling was required for the early expansion of *Ptpn2*-deficient cells (Fig. 5g) and the increased differentiation of *Ptpn2*-deleted cells into Tim-3$^+$ cells (Fig. 5h). Given PTPN2 regulates common signaling molecules, such as STAT1 and JAK1, within the type 1 and 2 IFN pathways[32,33], we examined whether IFN-γ was required for the increased Tim-3$^+$ subset differentiation of *Ptpn2*-deleted CD8$^+$ T cells during LCMV clone 13 infection. Following IFN-γ blockade, *Ptpn2*-deleted CD8$^+$ T cells still had significantly increased expansion and elevated Slamf6$^+$ to Tim-3$^+$ subset differentiation compared to control cells (Supplementary Fig. 5f and Fig. 5i), but were decreased in percentage compared to isotype-treated *Ptpn2*-deleted cells, indicating a nonessential role for IFN-γ in the generation of Tim-3$^+$ cells (Supplementary Fig. 5g). Overall, these findings indicate that IFN-I signaling plays a crucial role in the differentiation of *Ptpn2*-deleted cells into Tim-3$^+$ cells.

Loss of *Ptpn2* enhances Tim-3$^+$CD8$^+$ T cell differentiation in tumors. Given the importance of dysfunctional T cell subpopulations in tumors[4,18,22–27], we next asked whether *Ptpn2* also regulates the balance and functions of CD8$^+$ T subpopulations in responses to tumors. We cotransferred congenically marked naive OT-1 TCR transgenic (specific for the ovalbumin (OVA) CD8 epitope $OVA_{257–264}$) *Ptpn2*-deleted and control CD8$^+$ T cells to wild-type recipients and subsequently challenged these mice with MC38-OVA tumors. Consistent with chronic LCMV infection, *Ptpn2*-deleted OT-1 CD8$^+$ T cells significantly outcompeted control CD8$^+$ T cells at day 7 in the tumor (Fig. 6a,b and Supplementary Fig. 6a). *Ptpn2* deletion also led to an increase in CD25 and a decrease in CD127 expression in transferred CD8$^+$ T cells in the tumor-draining lymph node (Supplementary Fig. 6b,c), indicating increased activation of these cells. In addition, *Ptpn2*-deleted cells had increased generation of IFN-γ$^+$TNF$^-$ cells following peptide restimulation in vitro (Supplementary Fig. 6d). Transcriptional profiling of control or *Ptpn2*-deleted CD8$^+$ T cells revealed that *Ptpn2*-deleted CD8$^+$ T cells were significantly enriched for the tumor infiltrating lymphocytes (TIL) Tim-3$^+$ signature, whereas control cells were enriched for the TIL Slamf6$^+$ signature (Fig. 6c and Supplementary Table 3) (ref. [4]). In addition, *Ptpn2*-deleted cells were significantly enriched for mTORC1 signaling and several other effector-related signatures that were also enriched in the *Ptpn2*-deleted cells in the LCMV model (Fig. 6d). Consistent with this, *Ptpn2* deletion increased the percentages of granzyme B-expressing OT-1 CD8$^+$ T cells in the tumor, draining lymph node and spleen, compared to control OT-1 CD8$^+$ T cells (Fig. 6e). To determine the functional effect of these cells, we transferred control or *Ptpn2*-deleted OT-1 CD8$^+$ T cells to recipient mice implanted with B16-OVA tumors (Fig. 6f). *Ptpn2*-deleted CD8$^+$ T cells had a significant effect on B16-OVA tumor growth and led to clearance of 25% of the tumors (Fig. 6g,h). Moreover, when control and *Ptpn2*-deleted cells were cotransferred in the B16-OVA model, *Ptpn2*-deleted OT-1 T cells had an increased percentage of the Slamf6$^-$Tim-3$^+$ subset compared to control cells (Fig. 6i). Thus, concordant with the LCMV clone 13 model, *Ptpn2*-deleted CD8$^+$ T cells outcompete control cells in the tumor, have elevated Tim-3 and granzyme B expression and possess increased effector function.

Deletion of *Ptpn2* enhances CD8$^+$ T cell responses to tumors and checkpoint blockade efficacy. PTPN2 is ubiquitously expressed in the hematopoietic compartment and has roles in myeloid, T and B cell development and function[34]. Thus, therapeutic targeting of PTPN2 could potentially affect multiple immune subtypes. To model this, we investigated whether *Ptpn2* deletion in all hematopoietic cells would attenuate tumor growth by subcutaneously implanting MC38 tumors directly into the chimeras (Fig. 7a and

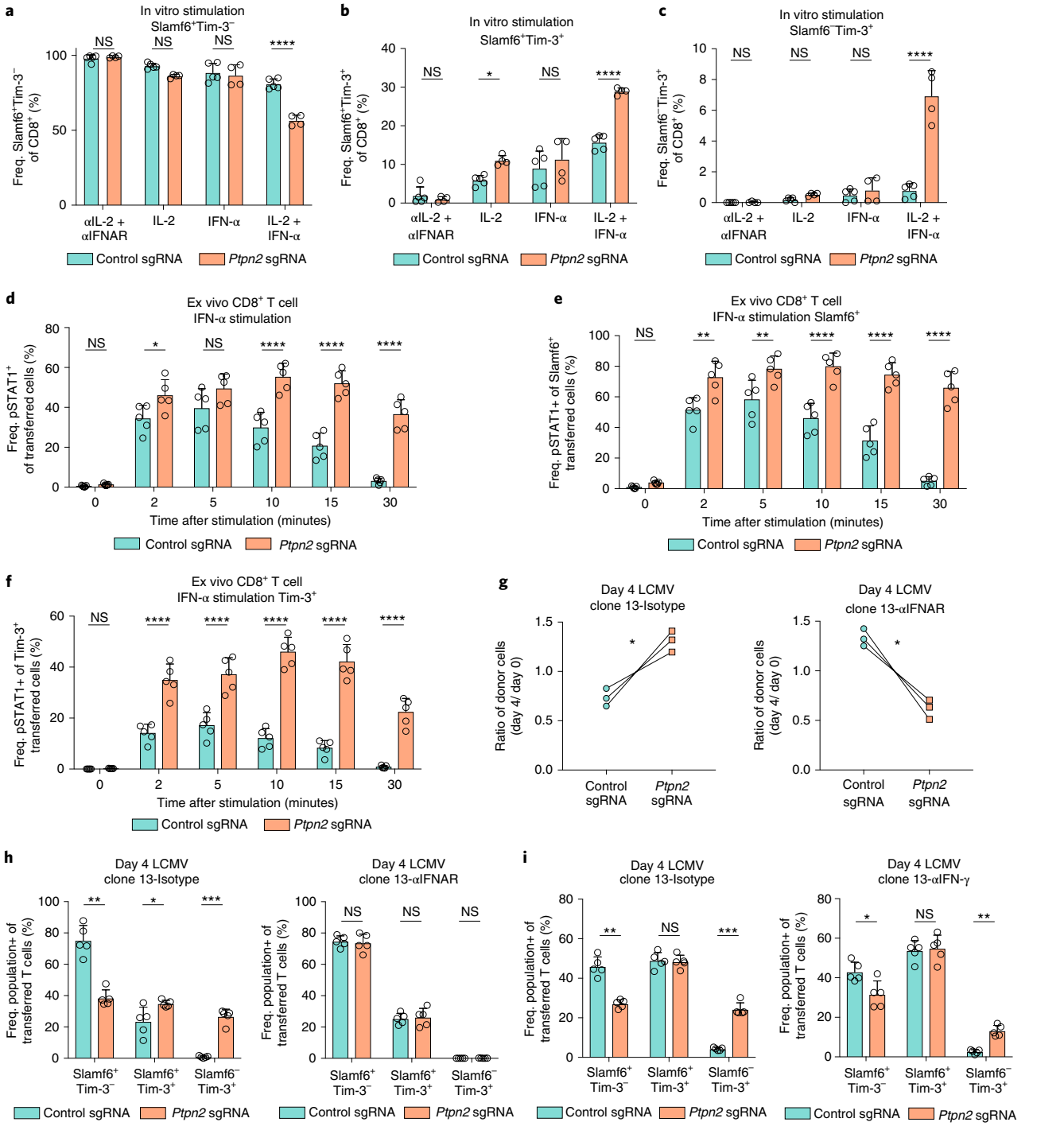

Fig. 5 | *Ptpn2* deletion increases Tim-3⁺ cell differentiation through enhanced IFN-α signaling. a–**c**, Quantification of Slamf6⁺Tim-3⁻ (**a**), Slamf6⁺Tim-3⁺ (**b**) and Slamf6⁻Tim-3⁺ (**c**) subsets following in vitro stimulation (anti-CD3/CD28) of control or *Ptpn2*-deleted naive CD8⁺ T cells in the presence of indicated cytokines or blocking antibodies. Data are representative of two pooled experiments, $n \geq 4$ technical replicates. **d**, Quantification of pSTAT1 expression of splenic CD8⁺ T cells 6 d after LCMV clone 13 infection for cotransferred control and *Ptpn2*-deleted cells following ex vivo restimulation with IFN-α. Data are representative of two independent experiments, $n = 5$ biological replicates. **e**,**f**, Quantification of pSTAT1 in Slamf6⁺ (**e**) or Tim-3⁺ cells (**f**) following ex vivo IFN-α restimulation of cotransferred control and *Ptpn2*-deleted cells as in **d**. Data are representative of two independent experiments, $n = 5$ biological replicates. **g**, Quantification of frequencies of cotransferred control and *Ptpn2*-deleted CD8⁺ T cells 4 d after LCMV clone 13 infection following treatment with isotype (left graph) or IFNAR blocking antibody (right graph). Frequencies at day 4 were normalized to input frequencies at day 0. Data are representative of two independent experiments, $n = 3$ biological replicates. **h**, Quantification of Slamf6⁺Tim-3⁻, Slamf6⁺Tim-3⁺ and Slamf6⁻Tim-3⁺ subsets 4 d after LCMV clone 13 infection in mice that received cotransferred control and *Ptpn2*-deleted P14 CD8⁺ T cells and were treated with isotype (left) or IFNAR blocking antibody (right). Data are representative of two independent experiments, $n = 5$ biological replicates. **i**, Quantification of Slamf6⁺Tim-3⁻, Slamf6⁺Tim-3⁺ and Slamf6⁻Tim-3⁺ subsets 4 d after LCMV clone 13 infection in mice that received cotransferred control and *Ptpn2*-deleted P14 CD8⁺ T cells and were treated with isotype (left) or IFN-γ neutralizing antibody (right). Data are representative of two independent experiments, $n = 5$ biological replicates. Bar graphs represent the mean and error bars represent the s.d. Statistical significance was assessed by two-way ANOVA (**a**–**c**) or two-sided Student's paired *t*-test (**d**–**i**) (NS, $P > 0.05$, $^{*}P \leq 0.05$, $^{**}P \leq 0.01$, $^{***}P \leq 0.001$, $^{****}P \leq 0.0001$). See also Supplementary Fig. 5.

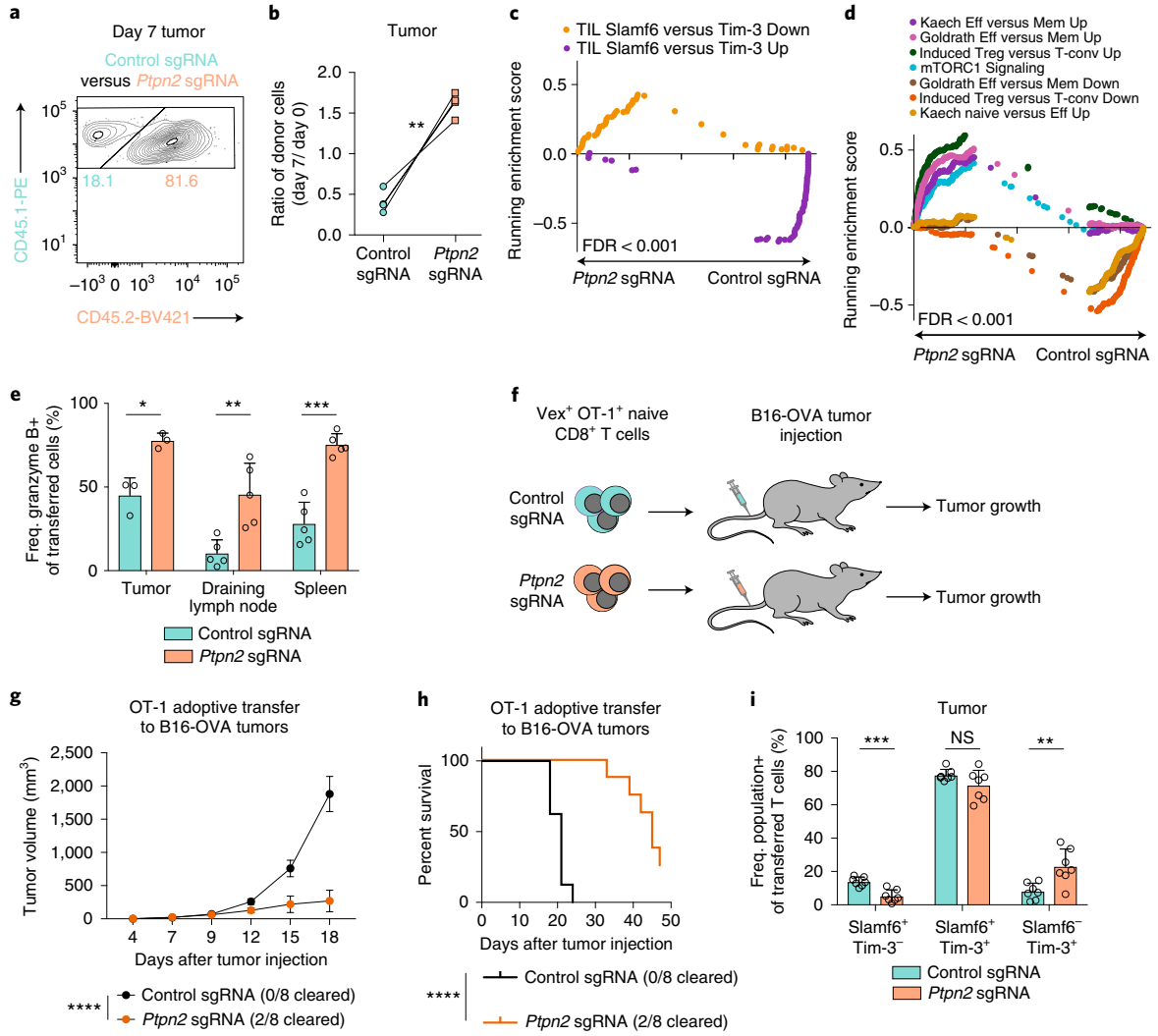

Fig. 6 | Loss of *Ptpn2* enhances Tim-3⁺ CD8⁺ T cell differentiation in tumors. a, Representative flow cytometry plot of control or *Ptpn2*-deleted OT-1 T cells in the tumor 7 d after MC38-OVA injection. Data are representative of two independent experiments, $n = 4$ biological replicates. **b**, Quantification of frequencies of cotransferred control or *Ptpn2*-deleted CD8⁺ T cells 7 d after MC38-OVA injection. Frequencies at day 7 were normalized to input frequencies at day 0. Data are representative of two independent experiments, $n = 4$ biological replicates. **c**,**d**, GSEA TIL Slamf6⁺ versus Tim-3⁺ Up top 50 and TIL Slamf6⁺ versus Tim-3⁺ Down top 50 signature enrichment (**c**) and GSEA effector signatures for cotransferred control or *Ptpn2*-deleted OT-1 T cells in MC38-OVA tumors (**d**) 7 d after injection. Data are representative of one experiment, $n = 3$ pooled mice and two technical replicates. **e**, Quantification of granzyme B expression in cotransferred OT-1 CD8⁺ T cells 7 d after MC38-OVA implantation in the tumor, draining lymph node and spleen for control and *Ptpn2*-deleted cotransferred mix as in **a**. Data are representative of two independent experiments, $n \geq 3$ mice. **f**, Schematic of adoptive transfer of either control or *Ptpn2*-deleted naive OT-1 CD8⁺ T cells separately to mice challenged with B16-OVA 1 d after transfer of T cells. **g**, Tumor growth curves for B16-OVA tumors following transfer of naive OT-1 control or *Ptpn2*-deleted CD8⁺ T cells separately into wild-type recipients that were implanted with B16-OVA cells. Data are representative of two independent experiments, $n = 8$ mice. **h**, Survival curves of mice in **g**. Data are representative of two independent experiments, $n = 8$ mice. **i**, Quantification of Slamf6⁺Tim-3⁻, Slamf6⁺Tim-3⁺ and Slamf6⁻Tim-3⁺ subsets 9 d after B16-OVA implantation in the tumor for cotransferred control and *Ptpn2*-deleted cells as in **a**. Data are representative of two independent experiments, $n = 7$ mice. Bar graphs represent the mean and error bars represent the s.d. (except for **g**, where error bars represent the s.e.m.). Statistical significance was assessed by a two-sided Student's paired *t*-test (**b**,**e**,**i**), two-sided Kolmogorov–Smirnov test (**c**,**d**), two-way ANOVA (**g**) or two-sided log-rank Mantel–Cox test (**h**) (NS, $P > 0.05$, $^{*}P \leq 0.05$, $^{**}P \leq 0.01$, $^{***}P \leq 0.001$, $^{****}P \leq 0.0001$). See also Supplementary Fig. 6. Panel **f** adapted from ref. [28], Springer Nature Ltd.

Supplementary Fig. 7a). Given PTPN2 has a role in myeloid and regulatory T cells[35,36], we examined these cell types in the blood of the chimeras at steady state and found similar frequencies of myeloid and regulatory T cell subsets in the blood, but elevated major histocompatibility complex (MHC)-II⁺ monocytes in the *Ptpn2*-deleted chimeras, compared to controls (Supplementary Fig. 7b). In addition, the *Ptpn2*-deleted chimeras did not have elevated inflammatory cytokine levels compared to controls (Supplementary Fig. 7c).

We next evaluated tumor growth in these chimeras and found that deletion of *Ptpn2* led to complete MC38 tumor clearance in all *Ptpn2*-deleted chimeras, whereas there was progressive tumor growth in control chimeras (Fig. 7b and Supplementary Fig. 7d). There were no differences in the absolute numbers of CD4⁺ T cells, CD8⁺ T cells and myeloid cells in the MC38 tumors before clearance (Supplementary Fig. 7e). However, the frequency and number of Slamf6⁻Tim-3⁺CD8⁺ T cells was increased in the tumors of *Ptpn2*-deficient chimeras compared to control chimeras (Fig. 7c,d),

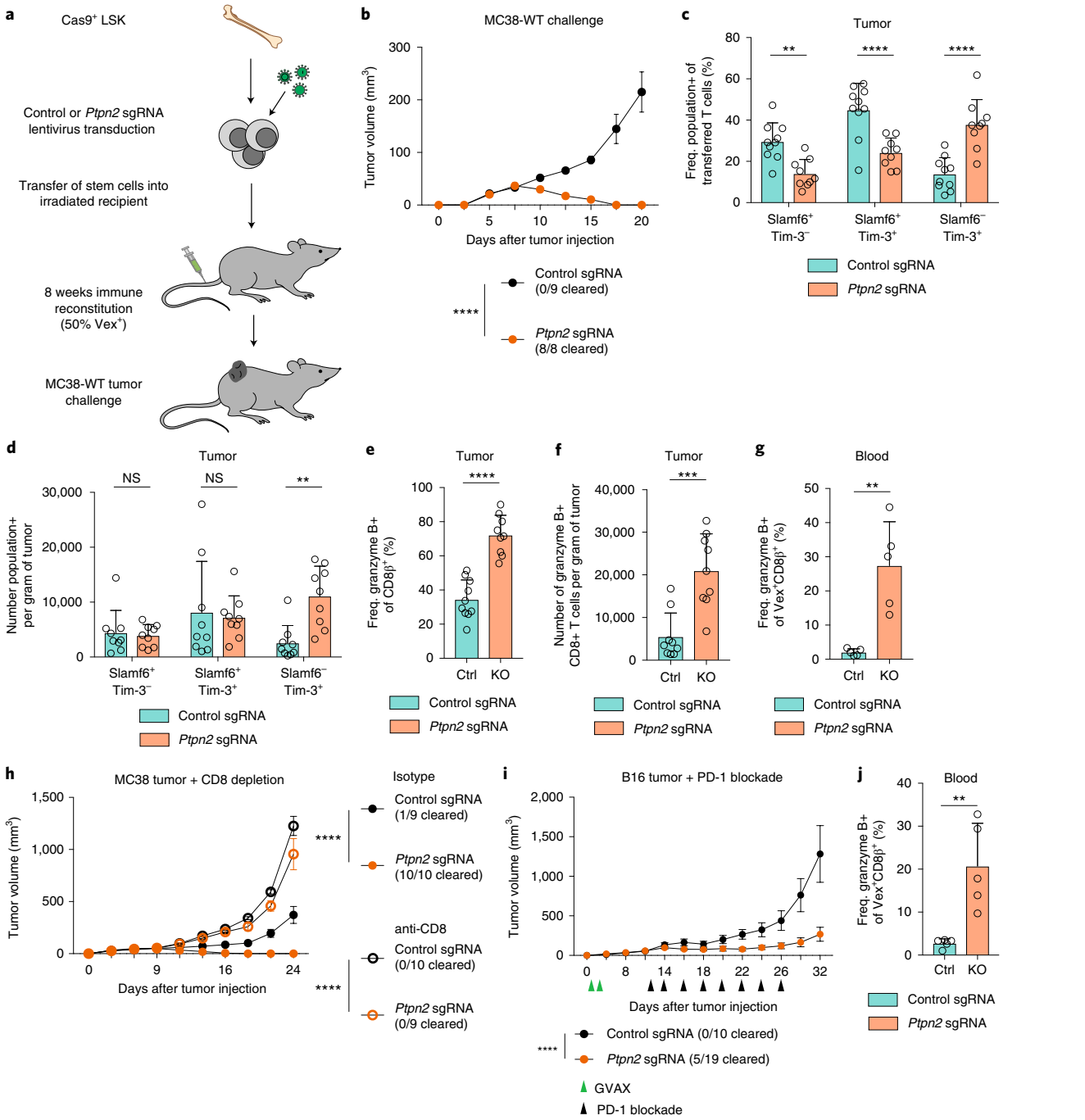

Fig. 7 | Deletion of *Ptpn2* enhances CD8⁺ T cell responses to tumors and checkpoint blockade efficacy. a, Schematic for MC38-WT tumor challenge in chimeric mice where approximately 50% of immune cells express a control sgRNA or a *Ptpn2*-targeting sgRNA. WT, wild type. **b**, Tumor growth curves for control or *Ptpn2*-deleted chimeric mice following 1×10^6 cell MC38-WT challenge. Representative of two independent experiments, $n\geq8$ mice. **c**,**d**, Quantification of frequency (**c**) and number of (**d**) Slamf6⁺Tim-3⁻, Slamf6⁺Tim-3⁺ and Slamf6⁻Tim-3⁺ subsets in CD8⁺ T cells infiltrating day 9 MC38 tumors in control or *Ptpn2*-deleted bone marrow chimeras. Data are representative of two independent experiments, $n\geq9$ mice. **e**,**f**, Quantification of frequency (**e**) and number of (**f**) granzyme B-expressing CD8⁺ T cells infiltrating day 9 MC38 tumors implanted in control or *Ptpn2*-deleted bone marrow chimeras. Data are representative of two independent experiments, $n\geq9$ mice. **g**, Quantification of frequency of granzyme B⁺ CD8⁺ T cells from the blood of control or *Ptpn2*-deleted bone marrow chimeras 14 d after MC38 tumor implantation, pre-gated on CD8β⁺Vex⁺ cells. Data are representative of two independent experiments, $n=5$ mice. **h**, Tumor growth curves for mice as in **a**, challenged with 1×10^6 MC38-WT tumor cells following treatment with CD8-depleting antibody or isotype control. Data are representative of two independent experiments, $n\geq9$ mice. **i**, Tumor growth curves for control or *Ptpn2*-deleted bone marrow chimeras challenged with 1×10^6 B16 tumor cells treated with GVAX (green triangles) on days 1, 4 and anti-PD-1 (black triangles) on days 12, 14, 16, 18, 20, 22, 24 and 26. Data are representative of two independent experiments, $n\geq9$ mice. **j**, Quantification of frequency of granzyme B⁺ CD8⁺ T cells from the blood of chimeras in **i**, 14 d after B16 tumor implantation, pre-gated on CD8β⁺Vex⁺ cells. Data are representative of two independent experiments, $n=5$ mice. Bar graphs represent the mean and error bars represent the s.d. (except for **b**,**h**,**i** where error bars represent the s.e.m.). Statistical significance was assessed by two-way ANOVA (**b**–**d**,**h**,**i**) or a two-sided Student's unpaired *t*-test (**e**–**g**,**j**) (NS, $P>0.05$, $^*P\leq0.05$, $^{**}P\leq0.01$, $^{***}P\leq0.001$, $^{****}P\leq0.0001$). See also Supplementary Fig. 7. Panel **a** adapted from ref. [28], Springer Nature Ltd.

whereas the number of Slamf6$^+$Tim-3$^-$CD8$^+$ T cells was unchanged. Furthermore, the frequency and number of granzyme B$^+$ CD8$^+$ T cells was also increased in tumors of *Ptpn2*-deficient chimeras compared to control chimeras (Fig. 7e,f). In addition, peripheral blood CD8$^+$ T cells of *Ptpn2*-deleted chimeras had significantly more granzyme B$^+$ cells, fewer CD127$^+$ cells, more Slamf6$^-$Tim-3$^+$ cells and more CD44$^+$CD62L$^-$ cells (Fig. 7g and Supplementary Fig. 7f–i). CD8$^+$ T depletion studies revealed that CD8$^+$ T cells are required for clearance of MC38 tumors in *Ptpn2*-deleted mice (Fig. 7h and Supplementary Fig. 7j). Furthermore, *Ptpn2*-deleted chimeras that completely eliminated primary tumors could clear a larger secondary challenge of MC38 tumor cells in a CD8$^+$ T cell-dependent manner (Supplementary Fig. 7k,l).

We next asked whether *Ptpn2* deficiency in the immune system could improve PD-1 ICB responses to a more immunorefractory model, B16 melanoma. Treatment of B16-challenged *Ptpn2*-deficient chimeras with PD-1 ICB and therapeutic vaccination (GVAX)[37] resulted in attenuated tumor growth and increased survival compared to control chimeras (Fig. 7i and Supplementary Fig. 7m). In addition, 26% of the anti-PD-1-treated *Ptpn2*-deleted chimeras completely cleared their tumors, in contrast to progressive tumor growth in all control chimeras. This enhanced response to B16 melanoma was accompanied by an increase in granzyme B$^+$ CD8$^+$ T cells in the peripheral blood (Fig. 7j). These findings demonstrate that *Ptpn2* deficiency in the immune system increases the cytotoxic CD8$^+$ T cell response in the tumor and ultimately leads to a CD8$^+$ T cell-dependent clearance of MC38 tumors and improved PD-1 ICB responses to B16 tumors.

Discussion

The mechanisms that govern the generation and balance of the terminally exhausted and progenitor exhausted subpopulations in chronic infection and cancer remain unknown. Here we demonstrate that deletion of *Ptpn2* in CD8$^+$ T cells enhances anti-tumor immunity by increasing the formation of the Tim-3$^+$ subset. We find at early and late time points that *Ptpn2* deletion promotes effector-related gene expression in both the progenitor (Slamf6$^+$) and terminally exhausted (Tim-3$^+$) subsets, indicating *Ptpn2* deletion alters both the balance and functionality of the exhausted subpopulations. Deletion of *Ptpn2* also promotes IFN-α signaling, which accelerates Tim-3$^+$ cell differentiation at an early time point. Furthermore, deletion of *Ptpn2* in the immune system leads to complete clearance of MC38 tumors and improves PD-1 ICB responses to B16 tumors. Overall, these findings improve our understanding of the differentiation and role of the Tim-3$^+$ subpopulation during anti-tumor immune responses.

Our work implicates PTPN2 as a new regulator of the balance between the Tim-3$^+$ and Slamf6$^+$ subpopulations. PTPN2 has a crucial effect on this balance primarily at early time points during LCMV clone 13 infection, where the Tim-3$^+$ and Slamf6$^+$ subpopulations differentiate from early effector cells into exhausted cells. PTPN2 has a multitude of targets to dephosphorylate within the TCR, IL-2, IL-7 and IFN signaling cascades[30,38]. Here we show that *Ptpn2* deletion leads to enhanced IFN-I signaling, which is required for the early competitive advantage seen in *Ptpn2*-deleted CD8$^+$ T cells, as well as the enhanced early differentiation of Slamf6$^+$Tim-3$^-$ cells into Slamf6$^+$Tim-3$^+$ and Slamf6$^-$Tim-3$^+$ cells. These findings are consistent with IFN-I signaling attenuating the TCF1–Bcl6 axis during LCMV infection, resulting in an increase in the percentage of Tim-3$^+$ cells[18], and highlight a crucial role for IFN-I signaling early in the differentiation of terminally exhausted cells[39,40]. We also find a nonessential role for IFN-γ signaling in promoting the differentiation of Tim-3$^+$ cells in *Ptpn2*-deleted CD8$^+$ T cells, as would be expected given its shared signaling pathway members with IFN-I. Additional studies will be needed to determine whether IFN-γ has a direct role on CD8$^+$ T cells or an indirect role on MHC-I expression in the host. Moreover, we find an essential role for IL-2 in vitro for enhancing Tim-3$^+$ subset formation in *Ptpn2*-deleted cells, where it likely works in conjunction with IFN-α to support proliferation[41]. This is consistent with a requirement for proliferation of CXCR5$^+$ progenitor cells to differentiate into Tim-3$^+$ terminally exhausted cells during LCMV clone 13 infection[17]. Overall, these findings help to elucidate the molecular mechanisms controlling CD8$^+$ T cell fate decisions into progenitor or terminally exhausted subpopulations in response to LCMV infection[42].

Currently, it is believed that an increase in the progenitor exhausted subpopulation promotes the efficacy of PD-1 ICB in chronic infection and cancer[4,16,17,24]. However, the Tim-3$^+$ subpopulation is the primary cytotoxic population[4,15], and thus also plays an important role in immune responses. It is likely that both progenitor exhausted and terminally exhausted cells are required for an effective immune response that balances cytotoxic potential and longevity. Our work represents a scenario where *Ptpn2* deletion causes an early increase in the cytotoxic Tim-3$^+$ subpopulation without altering the number of progenitor Slamf6$^+$ CD8$^+$ T cells. This occurs because: (1) *Ptpn2*-deleted Slamf6$^+$ cells have increased conversion into Tim-3$^+$ cells; (2) *Ptpn2*-deleted Slamf6$^+$ cells have increased proliferative capacity and thus can replenish the Slamf6$^+$ cell pool; and (3) *Ptpn2*-deleted Tim-3$^+$ cells have increased proliferative capacity, which further expands their numbers. This early increase in the number of cytotoxic cells and their inherent cytotoxic potential results in clearance of MC38 tumors and improved responses of B16 tumors to PD-1 blockade. These findings can be reconciled with data showing that an increase in the progenitor subpopulation improves checkpoint blockade responses by considering that following PD-1 blockade, the progenitor exhausted subpopulation expands and converts into terminally exhausted cytotoxic Tim-3$^+$ cells[4,16,17]. Our findings suggest that both the progenitor and terminally exhausted subpopulations can promote anti-tumor immunity and that *Ptpn2* deletion leads to improved tumor immunity through an increase in Tim-3$^+$ cytotoxic cells, without depleting the progenitor subpopulation.

Finally, this work supports the development of PTPN2 inhibitors for cancer immunotherapy and the deletion of *PTPN2* in chimeric antigen receptor T cell-based therapies. PTPN2 has a cell-intrinsic role in CD8$^+$ T cells in tumors, limiting their accumulation and expression of granzyme B, consistent with *Ptpn2*- deficient CD8$^+$ T cell responses in the LCMV model and the RIP-mOVA model of diabetes[43]. Moreover, adoptive transfer of *Ptpn2*-deleted CD8$^+$ T cells potently attenuates the growth of B16-OVA tumors, demonstrating that the increase in Tim-3$^+$ cells following *Ptpn2* deletion has a therapeutic benefit on tumor immunity. Furthermore, deletion of *Ptpn2* in the whole hematopoietic compartment leads to a CD8$^+$ T cell-dependent complete clearance of MC38 tumors, accompanied by a significantly elevated systemic cytotoxic CD8$^+$ T cell response, which could be beneficial for enhancing immunity to disseminated metastatic disease[44,45]. *Ptpn2* deletion in the immune system also improves PD-1 ICB responses to B16 tumors, indicating its potential use as a combination therapy with PD-1 blockade.

PTPN2 is a particularly attractive cancer immunotherapy target given its established tumor-intrinsic role in restraining anti-tumor immunity[46]. Inhibition of PTPN2 in a tumor-bearing host would enhance IFN-γ signaling within tumor cells, thereby increasing MHC-I expression and sensitivity to IFN-γ-mediated apoptosis[46]. Increased MHC-I expression would also promote TCR-driven differentiation of exhausted T cells into the Tim-3$^+$ population[4]. In addition, PTPN2 inhibition in CD8$^+$ T cells would increase IFN-I signaling and further enhance the formation and effector function of the cytotoxic Tim-3$^+$ population. Overall, these findings provide the rationale for combining PTPN2 inhibition and PD-1 ICB for cancer immunotherapy and for deletion of *PTPN2* in chimeric antigen receptor T cell therapies.

Online content

Any methods, additional references, Nature Research reporting summaries, source data, statements of code and data availability and associated accession codes are available at https://doi.org/10.1038/s41590-019-0480-4.

Received: 11 February 2019; Accepted: 29 July 2019;
Published online: 16 September 2019

References

1. Zajac, A. J. et al. Viral immune evasion due to persistence of activated T cells without effector function. *J. Exp. Med.* **188**, 2205–2213 (1998).
2. Wherry, E. J. T cell exhaustion. *Nat. Immunol.* **12**, 492–499 (2011).
3. Baitsch, L. et al. Exhaustion of tumor-specific CD8(+) T cells in metastases from melanoma patients. *J. Clin. Invest.* **121**, 2350–2360 (2011).
4. Miller, B. C. et al. Subsets of exhausted CD8(+) T cells differentially mediate tumor control and respond to checkpoint blockade. *Nat. Immunol.* **20**, 326–336 (2019).
5. Wherry, E. J., Blattman, J. N., Murali-Krishna, K., van der Most, R. & Ahmed, R. Viral persistence alters CD8 T-cell immunodominance and tissue distribution and results in distinct stages of functional impairment. *J. Virol.* **77**, 4911–4927 (2003).
6. Day, C. L. et al. PD-1 expression on HIV-specific T cells is associated with T-cell exhaustion and disease progression. *Nature* **443**, 350–354 (2006).
7. Wherry, E. J. et al. Molecular signature of CD8+ T cell exhaustion during chronic viral infection. *Immunity* **27**, 670–684 (2007).
8. Angelosanto, J. M., Blackburn, S. D., Crawford, A. & Wherry, E. J. Progressive loss of memory T cell potential and commitment to exhaustion during chronic viral infection. *J. Virol.* **86**, 8161–8170 (2012).
9. Doering, T. A. et al. Network analysis reveals centrally connected genes and pathways involved in CD8+ T cell exhaustion versus memory. *Immunity* **37**, 1130–1144 (2012).
10. Sen, D. R. et al. The epigenetic landscape of T cell exhaustion. *Science* **354**, 1165–1169 (2016).
11. Pauken, K. E. et al. Epigenetic stability of exhausted T cells limits durability of reinvigoration by PD-1 blockade. *Science* **354**, 1160–1165 (2016).
12. Shin, H. & Wherry, E. J. CD8 T cell dysfunction during chronic viral infection. *Curr. Opin. Immunol.* **19**, 408–415 (2007).
13. Utzschneider, D. T. et al. High antigen levels induce an exhausted phenotype in a chronic infection without impairing T cell expansion and survival. *J. Exp. Med.* **213**, 1819–1834 (2016).
14. Cornberg, M. et al. Clonal exhaustion as a mechanism to protect against severe immunopathology and death from an overwhelming CD8 T cell response. *Front. Immunol.* **4**, 475 (2013).
15. Paley, M. A. et al. Progenitor and terminal subsets of CD8+ T cells cooperate to contain chronic viral infection. *Science* **338**, 1220–1225 (2012).
16. He, R. et al. Follicular CXCR5-expressing CD8(+) T cells curtail chronic viral infection. *Nature* **537**, 412–428 (2016).
17. Im, S. J. et al. Defining CD8+ T cells that provide the proliferative burst after PD-1 therapy. *Nature* **537**, 417–421 (2016).
18. Wu, T. et al. The TCF1-Bcl6 axis counteracts type I interferon to repress exhaustion and maintain T cell stemness. *Sci. Immunol.* **1**, eaai8593–eaai8593 (2016).
19. Shan, Q. et al. The transcription factor Runx3 guards cytotoxic CD8(+) effector T cells against deviation towards follicular helper T cell lineage. *Nat. Immunol.* **18**, 931–939 (2017).
20. Snell, L. M. et al. CD8(+) T cell priming in established chronic viral infection preferentially directs differentiation of memory-like cells for sustained immunity. *Immunity* **49**, 678–694 e675 (2018).
21. Danilo, M., Chennupati, V., Silva, J. G., Siegert, S. & Held, W. Suppression of Tcf1 by inflammatory cytokines facilitates effector CD8 T cell differentiation. *Cell Rep.* **22**, 2107–2117 (2018).
22. Philip, M. et al. Chromatin states define tumour-specific T cell dysfunction and reprogramming. *Nature* **545**, 452–456 (2017).
23. Brummelman, J. et al. High-dimensional single cell analysis identifies stem-like cytotoxic CD8(+) T cells infiltrating human tumors. *J. Exp. Med.* **215**, 2520–2535 (2018).
24. Sade-Feldman, M. et al. Defining T cell states associated with response to checkpoint immunotherapy in melanoma. *Cell* **175**, 998–1013.e1020 (2018).
25. Thommen, D. S. et al. A transcriptionally and functionally distinct PD-1(+) CD8(+) T cell pool with predictive potential in non-small-cell lung cancer treated with PD-1 blockade. *Nat. Med.* **24**, 994–1004 (2018).
26. Siddiqui, I. et al. Intratumoral Tcf1(+)PD-1(+)CD8(+) T cells with stem-like properties promote tumor control in response to vaccination and checkpoint blockade immunotherapy. *Immunity* **50**, 195–211 e110 (2019).
27. Kurtulus, S. et al. Checkpoint blockade immunotherapy induces dynamic changes in PD-1(-)CD8(+) tumor-infiltrating T cells. *Immunity* **50**, 181–194 e186 (2019).
28. LaFleur, M. W. et al. A CRISPR-Cas9 delivery system for in vivo screening of genes in the immune system. *Nat. Commun.* **10**, 1668 (2019).
29. Brinkman, E. K., Chen, T., Amendola, M. & van Steensel, B. Easy quantitative assessment of genome editing by sequence trace decomposition. *Nucleic Acids Res.* **42**, e168 (2014).
30. Wiede, F. et al. T cell protein tyrosine phosphatase attenuates T cell signaling to maintain tolerance in mice. *J. Clin. Invest.* **121**, 4758–4774 (2011).
31. Curtsinger, J. M., Valenzuela, J. O., Agarwal, P., Lins, D. & Mescher, M. F. Cutting edge: type I IFNs provide a third signal to CD8 T cells to stimulate clonal expansion and differentiation. *J. Immunol.* **174**, 4465–4469 (2005).
32. ten Hoeve, J. et al. Identification of a nuclear Stat1 protein tyrosine phosphatase. *Mol. Cell Biol.* **22**, 5662–5668 (2002).
33. Simoncic, P. D., Lee-Loy, A., Barber, D. L., Tremblay, M. L. & McGlade, C. J. The T Cell Protein tyrosine phosphatase is a negative regulator of janus family kinases 1 and 3. *Curr. Biol.* **12**, 446–453 (2002).
34. Doody, K. M., Bourdeau, A. & Tremblay, M. L. T-cell protein tyrosine phosphatase is a key regulator in immune cell signaling-lessons from the knockout mouse model and implications in human disease. *Immunol. Rev.* **228**, 325–341 (2009).
35. Spalinger, M. R. et al. PTPN2 regulates inflammasome activation and controls onset of intestinal inflammation and colon cancer. *Cell Rep.* **22**, 1835–1848 (2018).
36. Svensson, M. N. et al. Reduced expression of phosphatase PTPN2 promotes pathogenic conversion of Tregs in autoimmunity. *J. Clin. Invest.* **129**, 1193–1210 (2019).
37. Dranoff, G. et al. Vaccination with irradiated tumor cells engineered to secrete murine granulocyte-macrophage colony-stimulating factor stimulates potent, specific, and long-lasting anti-tumor immunity. *Proc. Natl Acad. Sci. USA* **90**, 3539–3543 (1993).
38. Kleppe, M. et al. Deletion of the protein tyrosine phosphatase gene PTPN2 in T-cell acute lymphoblastic leukemia. *Nat. Genet.* **42**, 530–535 (2010).
39. Wilson, E. B. et al. Blockade of chronic type I interferon signaling to control persistent LCMV infection. *Science* **340**, 202–207 (2013).
40. Teijaro, J. R. et al. Persistent LCMV infection is controlled by blockade of type I interferon signaling. *Science* **340**, 207–211 (2013).
41. Starbeck-Miller, G. R., Xue, H. H. & Harty, J. T. IL-12 and type I interferon prolong the division of activated CD8 T cells by maintaining high-affinity IL-2 signaling in vivo. *J. Exp. Med.* **211**, 105–120 (2014).
42. Hashimoto, M., Ahmed, R., Im, S. J. & Araki, K. Cytokine-mediated regulation of CD8 T-cell responses during acute and chronic viral infection. *Cold Spring Harb. Perspect. Biol.* **11**, a028464 (2019).
43. Wiede, F., Ziegler, A., Zehn, D. & Tiganis, T. PTPN2 restrains CD8(+) T cell responses after antigen cross-presentation for the maintenance of peripheral tolerance in mice. *J. Autoimmun.* **53**, 105–114 (2014).
44. Marabelle, A. et al. Depleting tumor-specific Tregs at a single site eradicates disseminated tumors. *J. Clin. Invest.* **123**, 2447–2463 (2013).
45. Zamarin, D. et al. Localized oncolytic virotherapy overcomes systemic tumor resistance to immune checkpoint blockade immunotherapy. *Sci. Transl. Med.* **6**, 226ra232–226ra232 (2014).
46. Manguso, R. T. et al. In vivo CRISPR screening identifies Ptpn2 as a cancer immunotherapy target. *Nature* **547**, 413–418 (2017).

Acknowledgements

We thank N. Collins (Dana-Farber Cancer Institute), C. Kadoch (Dana-Farber Cancer Institute), D. Vignali (University of Pittsburgh), E.J. Wherry (University of Pennsylvania) and G. Dranoff (Novartis Institutes for BioMedical Research) for sharing cancer cell lines and F. Zhang (Broad Institute of MIT and Harvard) for sharing loxP-STOP-loxP-Cas9 mice. This work was supported by funding from grant no. T32CA207021 from the National Cancer Institute to M.W.L., the 2016 AACR-Bristol-Myers Squibb Fellowship in Translational Immuno-oncology grant no. 16-40-15-MILL, National Center for Advancing Translational Sciences/National Institutes of Health Award no. KL2 TR002542, the Jane C. Wright, MD, Endowed Young Investigator Award from ASCO to B.C.M. and grant nos. P50CA101942 from the National Cancer Institute to G.J.F., U19AI133524 from the National Institute of Allergy and Infectious Diseases to A.H.S and W.N.H. and U54 CA225088 from the National Cancer Institute, R01 CA229851 from the National Cancer Institute and P01 AI108545 from the National Institute of Allergy and Infectious Diseases to A.H.S.

Author contributions

M.W.L., W.N.H. and A.H.S. conceived the project and wrote the manuscript with assistance from T.H.N., M.A.C., B.C.M., E.F.G., J.E.G. and G.J.F.. M.W.L., T.H.N., W.N.H. and A.H.S. designed experiments. M.W.L. and T.H.N. performed and analyzed all experiments with assistance from M.A.C., J.E.G. and E.F.G.. K.B.Y. performed bulk RNA-seq sample processing and analyzed the RNA-seq data. B.C.M. and R.A. performed 10× single-cell RNA-seq sample processing and analyzed the single-cell RNA-seq data. D.R.S. performed ATAC-seq sample processing and analyzed the ATAC-seq data. G.J.F. contributed to anti-PD-1 experiments.

Competing interests

A.H.S. has patents on the PD-1 pathway licensed by Roche/Genentech and Novartis, consults for Novartis, is on the scientific advisory boards for Surface Oncology, Sqz Biotech, Elstar Therapeutics, Elpiscience, Selecta and Monopteros and has research funding from Merck, Novartis, Roche, Ipsen, UCB and Quark Ventures. W.N.H. has a patent application on T cell exhaustion-specific enhancers held by the Dana-Farber Cancer Institute and now is employed by Merck. W.N.H. is also a founder of Arsenal Biosciences. A.H.S. and W.N.H. have a patent application on PTPN2 as a therapeutic target held/submitted by the Dana-Farber Cancer Institute. G.J.F. has a consulting or advisory role for Novartis, Lilly, Roche/Genentech, Bristol-Myers Squibb, Bethyl Laboratories, Xios Therapeutics, Quiet Therapeutics and Seattle Genetics; patents, royalties or other intellectual property from Novartis, Roche/Genentech, Bristol-Myers Squibb/Medarex, Amplimmune/Astrazeneca, Merck, EMD Serono and Boehringer Ingelheim and research funding from Bristol-Myers Squibb. The remaining authors declare no competing interests.

Additional information

Supplementary information is available for this paper at https://doi.org/10.1038/s41590-019-0480-4.

Correspondence and requests for materials should be addressed to W.N.H. or A.H.S.

Peer review information Zoltan Fehervari was the primary editor on this article and managed its editorial process and peer review in collaboration with the rest of the editorial team.

Methods

Mouse breeding and production. Seven- to ten-week-old female or male mice were used for all experiments and 7- to 14-week-old female or male mice were used as donors for bone marrow chimera experiments. Wild-type C57BL/6J mice were purchased from the Jackson Laboratory. LoxP-STOP-loxP-Cas9 mice (B6J.129(B6N)-Gt(ROSA) 26Sortm1(CAG-cas9*,-EGFP)Fezh/J)[47] were a generous gift from F. Zhang, Massachusetts Institute of Technology. These mice were bred to Zp3-Cre mice (C57BL/6-Tg(Zp3-cre)1Gwh/J) to delete the loxP-STOP-LoxP in the female germline. The resulting Cas9-expressing strain was then bred to OT-I (C57BL/6-Tg(TcraTcrb)1100Mjb/J) or P14 (Taconic B6.Cg-Tcratm1Mom Tg(TcrLCMV)327Sdz backcrossed ten generations to Jackson C57BL/6J) TCR transgenic mice on the CD45.1 (B6.SJL-Ptprca Pepcb/BoyJ) congenic background. All strains used were backcrossed at least ten generations to Jackson C57BL/6J. The sample size was chosen to ensure the possibility of statistical analysis and minimize the use of animals. Data exclusion was not used. Age and sex-matched animals were used for each experiment. For chimerism experiments, LSK donor, LSK recipients and CD8$^+$ T cell transfer recipients were sex-matched. Animals were also co-housed when possible. All attempts to reproduce our findings were successful. The LCMV clone 13 infection, MC38 tumor and B16 tumor experiments (Figs. 4i, 5g–i, 6g,h, 7b–j and Supplementary Figs. 2f, 4e,f, 5f,g, 7d–m) were blinded during data collection. All experimental mice were housed in specific pathogen-free conditions and used in accordance with animal care guidelines from the Harvard Medical School Standing Committee on Animals and the National Institutes of Health.

Guide RNA design and cloning. The sgRNA oligonucleotides (controls: GCGAGGTATTCGGCTCCGCG, GCTTTCACGGAGGTTCGACG and *Ptpn2*: GAATATGAGAAAGTATCGAA, CTCACTTCCATTATACCACC), were designed using the Broad CRISPR algorithm[48]. sgRNAs were cloned into our sgRNA vector using a BsmBI restriction digest. The plasmid and full sequence have been deposited on Addgene (Name: pXPR_053, Addgene ID: 113591).

Bone marrow isolation and chimera set-up. Bone marrow cells were isolated and cultured as previously described[28]. In short, femurs, tibias, hips and spines were isolated from donor mice, crushed and lysed with ammonium–chloride–potassium (ACK) lysing buffer (Gibco catalog no. A1049201). LSK cells (lineage$^-$ Sca-1$^+$ Kit$^+$) were enriched with a CD117 MACS isolation kit (Miltenyi catalog no. 130-091-224) and then sorted to purity. The LSK cells were spin transduced with lentiviral vectors on retronectin-coated plates (Takara Bio catalog no. T100B) at a multiplicity of infection of 25. LSK cells were then transferred intravenously into irradiated CD45.2$^+$ wild-type recipients.

Cell lines. MC38-OVA (a gift from N. Collins, Dana-Farber Cancer Institute), B16-OVA (a gift from D. Sen, Dana-Farber Cancer Institute), MC38-WT (a gift from D. Vignali, University of Pittsburgh School of Medicine), B16.F10 and B16/granulocyte–macrophage colony-stimulating factor (GM-CSF) (both gifts from G. Dranoff, Novartis Institutes for Biomedical Research), 293x (a gift from C. Kadoch, Dana-Farber Cancer Institute) and MC38-GP$_{33–41}$ cells[49] were cultured in DMEM supplemented with 10% FBS, 1% penicillin/streptomycin and 20 μg ml^{-1} gentamicin. MC38-OVA and B16-OVA cells were produced by transduction of parental MC38 and B16.F10 cells with the lentiviral vector TRC-pLX305 (Broad Institute) containing OVA protein. MC38-OVA and B16-OVA cells were selected for 2 d with 2 μg ml^{-1} puromycin before use to ensure expression of OVA (construct is OVA IRES puromycin resistance). MC38-GP$_{33–41}$ cells were monitored for expression of green fluorescent protein (GFP) to ensure expression of GP$_{33–41}$ peptide (construct is GP$_{33–41}$ IRES GFP). GM-CSF secretion by B16/GM-CSF cells was validated by ELISA. Parental MC38 and B16.F10 cell lines were validated by exome sequencing. BHK-21 cells (gift from E.J. Wherry, University of Pennsylvania) were cultured in DMEM supplemented with 10% FBS, 1% penicillin/streptomycin and 5% tryptose phosphate broth. Vero cells (a gift from E.J. Wherry, University of Pennsylvania) were cultured in EMEM supplemented with 10% FBS and 1% penicillin/streptomycin. All cell lines were confirmed as mycoplasma negative.

TIDE assay. The TIDE assay was performed as previously described[29]. Briefly, DNA was extracted from cells (DNeasy Blood and Tissue kit, QIAgen catalog no. 69506) and PCR was used to amplify the expected sgRNA target site, which was then purified (QIAquick PCR Purification kit, QIAgen catalog no. 28106) and analyzed by Sanger sequencing. TIDE primers used for respective sgRNAs (sgRNA-1 forward: GGGCACTGAGCAGCAAACTTTAT; sgRNA-1 reverse: GTGACTAGCTTTCA TCTTTGCCTCTT; sgRNA-2 forward: CTGGAAGGCTGGCTGTAGTGTT; sgRNA-2 reverse: CTAACCTCCTCAGGCACCAGTC).

Antibodies used for flow cytometry and sorting. Flow cytometry analyses were performed on a BD LSR II or BD FACSymphony and cell sorting was performed on a BD Aria II. Antibodies and dyes were purchased from BD Biosciences (7-AAD catalog no. 559925 (1:100 dilution), Slamf6 clone 13G3 catalog no. 561540 (1:100 dilution), BrdU clone 3D4 catalog no. 552598 (1:50 dilution), Ki-67-PerCP-Cy5.5 clone B56 catalog no. 561284 (1:100 dilution)); Biolegend (B220 clone RA3-6B2 catalog no. 103208, 103226 (1:100 dilution), CD11b clone M1/70 catalog no. 101208, 101216 (1:100 dilution), CD127 clone A7R34 catalog no. 135014, 135024 (1:100 dilution), CD25 clone PC61 catalog no. 101904 (1:100 dilution), CD3ε clone 17A2 catalog no. 100220, 100308, 100336, 100328 (1:100 dilution), CD4 clone RM4-5 catalog no. 100516, 100531, 100543 (1:100 dilution), CD44 clone IM7 catalog no. 103008, 103028, 103030 (1:100 dilution), CD45.1 clone A20 catalog no. 110708, 110716, 110741 (1:100 dilution), CD45.2 clone 104 catalog no. 109824, 109832, 109830 (1:100 dilution), CD5 clone 53-7.3 catalog no. 100608 (1:100 dilution), CD62L clone MEL-14 catalog no. 104417 (1:100 dilution), CD8α clone 53-6.7 catalog no. 100737 (1:100 dilution), CD8β clone YTS156.7.7 catalog no. 126606, 126608, 126610, 126620, 126614 (1:100 dilution), c-Kit clone ACK2 catalog no. 135108 (1:100 dilution), CXCR5 clone L138D7 catalog no. 145509 (1:50 dilution), Gr-1 clone RB6-8C5 catalog no. 108408 (1:100 dilution), granzyme B clone GB11 catalog no. 515403, 515406 (1:100 dilution), I-A/I-E clone M5/114.15.2 catalog no. 107614 (1:100 dilution), IFN-γ clone XMG1.2 catalog no. 505810 (1:100 dilution), IFNAR1 clone MAR1-5A3 catalog no. 127314 (1:100 dilution), Ly6c clone HK1.4 catalog no. 128007 (1:100 dilution), PD-1 clone 29F.1A12 catalog no. 135206, 135209 (1:100 dilution), Sca-1 clone D7 catalog no. 108108, 108128 (1:100 dilution), TCR Vα2 clone B20.1 catalog no. 127814, 127806 (1:100 dilution), TCR Vβ5 clone MR9-4 catalog no. 139506 (1:100 dilution), TCR Vβ8 clone KJ16-133.18 catalog no. 118406 (1:100 dilution), TER-119 clone TER-119 catalog no. 116208 (1:100 dilution), TCF1 clone 7F11A10 catalog no. 655208 (1:100 dilution), Tim-3 clone RMT3-23 catalog no. 119703, 119723 (1:100 dilution), TNF clone MP6-XT22 catalog no. 506322 (1:100 dilution), TruStain fcX clone 93 catalog no. 101320 (1:50 dilution), Rat IgG2a κ Isotype clone RTK2758 catalog no. 400508 (1:100 dilution), Rat IgG2b κ Isotype clone RTK4530 catalog no. 400612 (1:100 dilution), Streptavidin catalog no. 405225 (1:400)); Invitrogen anti-GFP (polyclonal) catalog no. A21311 (1:350 dilution); Thermo Fisher Scientific (Foxp3 clone FJK-16s catalog no. 48-5773-82 (1:50 dilution), Near-IR Fixable Live/Dead catalog no. L34976 (1:500 dilution)); and Cell Signaling Technology pSTAT1 clone 58D6 catalog no. 9174 (1:100 dilution).

Adoptive T cell transfer. Spleens were isolated from chimeric mice (>8 weeks after reconstitution) and naive CD8$^+$ T cells were purified using a naive CD8$^+$ MACS kit (Miltenyi catalog no. 130-096-543, >95% purity). Cells were stained with lineage-specific antibodies (TER-119, B220 and Gr-1) and 7-Aminoactinomycin D (7-AAD) and then sorted (Lineage$^-$, 7-AAD$^-$, Vex$^+$ cells). For LCMV cotransfer studies, cells were transferred (500:500 mix) to recipient mice on day −1, and mice were infected with LCMV clone 13 (as below) on day 0. For tumor cotransfer studies, cells were transferred (1000:1000 mix) to recipient mice on day −1, and mice were injected with MC38-OVA or B16-OVA (as below) on day 0. For transfer studies to determine effects on tumor growth, either 5,000 control or *Ptpn2*-deleted CD8$^+$ T cells were transferred alone into wild-type recipients on day −1 and mice were injected with B16-OVA (as below) on day 0.

LCMV production and plaque assay. LCMV clone 13 virus was produced by infecting BHK-21 cells with an LCMV clone 13 stock at a multiplicity of infection of 0.01 and harvesting viral supernatants 48 h later. Viral titers were determined by plating diluted viral stocks on Vero cells with an agarose overlay. After 4 d, the Vero cells were stained with neutral red dye and plaques were quantified 14 h later.

LCMV infection and analysis. Mice were infected with 4×10^6 PFU LCMV clone 13 intravenously, monitored for weight loss and bled or euthanized at 8, 15, 22 or 30 d after infection for flow cytometry analyses. To deplete CD4$^+$ T cells, mice were injected intraperitoneally with 200 μg of anti-CD4 (GK1.5, BioXCell catalog no. BE0003-1) on days −1 and 1 (relative to LCMV clone 13 injection on day 0). To block IFNAR1, mice were injected intraperitoneally with 1 mg αIFNAR (MAR1-5A3, BioXCell catalog no. BE0241) or isotype (MOPC-21, BioXCell catalog no. BE0083) on days −1 and 1 (relative to LCMV clone 13 injection on day 0). To block IFN-γ, mice were injected intraperitoneally daily with 250 μg of anti-IFN-γ (XMG1.2 BioXCell catalog no. BE0055) or isotype (HRPN BioXCell catalog no. BE0088) on days 0–3 (relative to LCMV clone 13 injection on day 0).

Isolation of liver-infiltrating lymphocytes. Livers were excised, mechanically minced and filtered to a single-cell suspension. Lymphocytes were enriched on a Percoll gradient (VWR catalog no. 89428-524).

Tumor injection. Mice were anesthetized with 2.5% 2,2,2-tribromoethanol (Avertin, Sigma-Aldrich catalog no. T48402-25G) and injected in the flank subcutaneously with 2×10^6 MC38-OVA tumor cells (cotransfer experiments), or 1×10^6 MC38-WT tumor cells (chimera primary challenge). For secondary rechallenge experiments, chimeras were allowed to rest for 60 d after primary tumor clearance and then were rechallenged with 5×10^6 MC38-WT tumor cells on the opposite flank subcutaneously (as above). For B16.F10 experiments, mice were challenged with 1×10^6 B16.F10 tumor cells subcutaneously (day 0), followed by injections on the opposite flank of 1×10^6 irradiated B16/GM-CSF cells (days 1 and 4). Mice were then treated intraperitoneally with 100 μg of rat monoclonal anti-PD-1 (clone 29F.1A12) on days 12, 14, 16, 18, 20, 22, 24 and 26. For B16-

OVA experiments mice were challenged with 2.5×10^5 B16-OVA tumor cells subcutaneously. Tumors were measured every 2–3 d once palpable using a caliper. Tumor volume was determined by the volume formula for an ellipsoid: $1/2 \times D \times d^2$ where D is the longer diameter and d is the shorter diameter. Mice were euthanized when tumors ulcerated, reached 2 cm^3 or a body condition score >2 was observed. To deplete CD8$^+$ T cells, mice were injected intraperitoneally with 100 µg of anti-CD8β (53-5.8 BioXCell catalog no. BE0223) or isotype (HRPN BioXCell catalog no. BE0088) on days −3, 0, 3, 6 and 9 and 200 µg of anti-CD8α (2.43 BioXCell catalog no. BE0061) or isotype (LTF-2 BioXCell catalog no. BE0090) on days 12, 15, 18, 21 and 24 (relative to MC38 tumor injection on day 0). For depletion of CD8$^+$ T cells in secondary rechallenge experiments, mice were injected intraperitoneally with 100 µg of anti-CD8α (53-6.7 BioXCell catalog no. BE0004-1) or isotype (2A3 BioXCell catalog no. BE0089) on days −3, 0, 3, 6 and 9 (relative to MC38 rechallenge on day 0).

Tumor infiltrating lymphocyte isolation. Tumors were excised and mechanically minced. Tumors were then incubated in collagenase for 10 min at 37 °C. Lymphocytes were enriched using an Optiprep gradient (Sigma-Aldrich catalog no. D1556).

Monitoring of T cell responses in the blood. To monitor the stability of Vex transduction, mice were bled via the tail vein. Blood was then lysed twice using ACK lysis buffer, stained and analyzed by flow cytometry. For monitoring of T cell responses to LCMV infection or tumor, mice were anesthetized with isoflurane (Henry Schein catalog no. 029404), retro-orbitally bled, and lymphocytes were isolated by centrifugation at 400*g* on a histopaque-1083 gradient (Sigma-Aldrich catalog no. 10831-6X100ML) and stained for flow cytometry.

In vitro T cell differentiation assay using naive CD8$^+$ T cells. Naive CD8$^+$ T cells were obtained from spleens of control and *Ptpn2*-deleted chimeric mice as described above. Naive CD8$^+$ T cells were then activated on plate-bound anti-CD3 (OKT-3, BioXCell catalog no. BE0001) (5 µg ml^{-1}) with or without anti-CD28 (37.51, BioXCell catalog no. BE00015) (5 µg ml^{-1}) and supplemented with 200 U ml^{-1} IL-2 (R&D Systems catalog no. 202-IL), 1000 U ml^{-1} IFN-α (PBL Assay Science catalog no. 12105-1), 50 µg ml^{-1} anti-IL-2 (S4B6-1, JES61A12, BioXCell catalog no. BE0043-1, BE0043) or 50 µg ml^{-1} anti-IFNAR blocking antibodies for 72 h. For supernatant transfer experiments, supernatant was isolated from wells of control or *Ptpn2*-deleted stimulated cells (72 h poststimulation as above). The supernatant was added to wild-type naive CD8$^+$ T cells activated on plate-bound anti-CD3 (5 µg ml^{-1}) and anti-CD28 (5 µg ml^{-1}) and supplemented with 200 U ml^{-1} IL-2, 1,000 U ml^{-1} IFN-α, 50 µg ml^{-1} anti-IL-2 or 50 µg ml^{-1} anti-IFNAR blocking antibodies for 72 h.

In vitro cytotoxicity assay using antigen-experienced Tim-3$^+$ CD8$^+$ T cells. Naive P14 control and *Ptpn2*-deleted CD8$^+$ T cells were cotransferred to wild-type recipient mice (500:500 mix) on day −1, and the mice were infected with LCMV clone 13 on day 0 (as above). CD4$^+$ T cells were depleted on days −1 and 1 (as above). Splenocytes were isolated on day 8 after infection and enriched for CD8$^+$ T cells using the CD8α$^+$ MACS kit (Miltenyi catalog no. 130-117-044). Vex$^+$ Tim-3$^+$CD8$^+$ T cells (Tim-3$^+$) or Vex$^+$CD8$^+$ T cells (bulk Slamf6$^+$ and Tim-3$^+$) were sorted from both control and *Ptpn2*-deleted cells. MC38-GP_{33-41}-GFP tumor cells were seeded with 20 ng ml^{-1} IFN-γ, 1 d before plating of the T cells. Tim-3$^+$ or bulk CD8$^+$ T cells were then cocultured with MC38-GP_{33-41}-GFP tumor cells at a 2:1 effector to target ratio for 16 h. After coculture, cells were trypsinized, stained and analyzed by flow cytometry to determine the number of remaining live tumor cells. The killing percentage was calculated by the formula:

100% × (1 – [no. live tumor cells in well with T cells / no. live tumor cells in well with no T cells])

In vitro T cell conversion assay using antigen-experienced Slamf6$^+$ CD8$^+$ T cells. Naive P14 control and *Ptpn2*-deleted CD8$^+$ T cells were cotransferred to wild-type recipient mice (500:500 mix) on day −1, and the mice were infected with LCMV clone 13 on day 0 (as above). CD4$^+$ T cells were depleted on days −1 and 1 (as above). Splenic control and *Ptpn2*-deleted CD8$^+$ T cells were isolated from cotransfer recipient mice and sorted for Slamf6$^+$Vex$^+$CD8$^+$ T cells. 50,000 Slamf6$^+$Vex$^+$CD8$^+$ T cells were stimulated on plate-bound anti-CD3 (5 µg ml^{-1}) and anti-CD28 (5 µg ml^{-1}), and were supplemented with 200 U ml^{-1} IL-2 and 1,000 U ml^{-1} IFN-α for 96 h. Cells were then stained and differentiation was assessed by flow cytometry.

In vitro CTV proliferation assay using antigen-experienced Slamf6$^+$ and Tim-3$^+$ CD8$^+$ T cells. Naive P14 control and *Ptpn2*-deleted CD8$^+$ T cells were cotransferred to wild-type recipient mice (500:500 mix) on day −1, and the mice were infected with LCMV clone 13 on day 0 (as above). CD4$^+$ T cells were depleted on days −1 and 1 (as above). Splenic control and *Ptpn2*-deleted CD8$^+$ T cells were isolated from cotransfer recipient mice and sorted for Slamf6$^+$Vex$^+$ CD8$^+$ T cells and Tim-3$^+$Vex$^+$CD8$^+$ T cells. These cells were labeled with 5 µM CTV proliferation dye (Thermo Fisher Scientific catalog no. C34557) for 20 min at 37 °C. 50,000 Slamf6$^+$ or Tim-3$^+$Vex$^+$CD8$^+$ T cells were stimulated on plate-bound anti-CD3 (0.5 µg ml^{-1}) and anti-CD28 (0.5 µg ml^{-1}) and were supplemented with 200 U ml^{-1} IL-2 for 72 h. Cells were then stained and proliferation was assessed by flow cytometry.

BrdU incorporation and detection. Mice were injected with 1 mg of BrdU intraperitoneally 16 h before euthanizing and analysis. Cells were processed and stained using the BrdU flow kit (BD Biosciences catalog no. 552598).

Ex vivo restimulation and flow cytometry of phosphorylated proteins. Naive P14 control and *Ptpn2*-deleted CD8$^+$ T cells were cotransferred to wild-type recipient mice (500:500 mix) on day −1, and the mice were infected with LCMV clone 13 on day 0 (as above). CD4$^+$ T cells were depleted on days −1 and 1 (as above). Splenocytes were isolated on day 6 after infection and enriched for CD8$^+$ T cells using CD8α$^+$ MACS kit. CD8$^+$ T cells were stimulated on plate-bound anti-CD3 (10 µg ml^{-1}) and anti-CD28 (10 µg ml^{-1}) and with 1,000 U ml^{-1} IFN-α for 0, 2, 5, 10, 15 and 30 min at 37 °C. After stimulation, cells were pelleted at 800*g*, fixed in 2% methanol-free formaldehyde (Cell Signaling Technology catalog no. 12606) and permeabilized with ice-cold 90% methanol for 20 min on ice. Cells were then washed with MACS buffer and stained with pSTAT1 antibody.

Quantification of serum cytokines. Serum was collected from control or *Ptpn2*-deleted chimeric mice 12 weeks after reconstitution. Inflammatory cytokines (IL-6, IL-10, MCP-1, IFN-γ, TNF and IL-12p70) were measured using a BD Cytometric Bead Assay Mouse Inflammation Kit (BD Biosciences catalog no. 552364).

ATAC-seq library preparation and analysis. 50,000 cotransferred control or *Ptpn2*-deleted Slamf6$^+$ or Tim-3$^+$ P14 T cells per replicate were sorted from spleens of day 8 LCMV clone 13-infected mice into PBS with 10% FBS. Pelleted cells were incubated in 50 µl of reaction mix (containing 2× Tagmentation DNA buffer, Tn5 enzyme and 2% digitonin in nuclease-free water) as previously described[50]. The transposase reaction was performed at 37 °C for 30 min with agitation at 300 r.p.m. DNA was then purified using a MinElute Reaction Cleanup kit (QIAgen catalog no. 28206). A post-PCR cleanup was performed using Agencourt AMPure XP beads (Beckman Coulter catalog no. A63880) and library quality was verified using Tapestation analysis. Samples were sequenced on an Illumina NextSeq500 sequencer using 37 base-pair paired-end reads.

Quality trimming and primer removal within raw fastq files were done with Trimmomatic 0.33 using the following parameters: LEADING: 15, TRAILING: 15, SLIDINGWINDOW: 4:15, MINLEN: 36. Trimmed reads were aligned to mm9 with Bowtie v.2.2.4 using a maximum insert size of 1,000. Aligned bams were sorted, duplicates marked, and reads mapping to the blacklist region were removed[51]. Peak-calling using MACS 2.1.1 was performed on merged bam files (Samtools v.1.3) from biological replicates using a q-value threshold of 0.001. Consensus peaks from all biological conditions were merged to create a single peak universe. Cut sites were extracted from each biological replicate and the number of cuts within each peak region were quantified to generate a raw count matrix. DESeq2 was used to normalize the counts matrix and perform differential accessibility analysis between all relevant comparisons. Tracks were visualized using Integrative Genomics Viewer v.2.3.77 (Broad Institute).

Bulk RNA-seq analysis of T cells. At day 7 or 8 after tumor or virus injection respectively, cotransferred T cells were isolated from the tumor or spleen (LCMV) (as above) and replicates of 500 cells were sorted into 25 µl of buffer RLT (QIAgen catalog no. 79216) + 1% beta-mercaptoethanol v/v. After flash-freezing on dry ice and storage at −80 °C, lysates were converted to cDNA following capture with Agencourt RNAClean beads (Beckman Coulter catalog no. A63987) using the SmartSeq2 protocol as previously described[52]. The cDNA was amplified using 16 PCR enrichment cycles before quantification and dual-index barcoding with the Illumina Nextera XT kit. The libraries were enriched with 12 cycles of PCR, then combined in equal volumes before final bead cleanup and sequencing on a NextSeq500 by 37 base-pair paired-end reads. After demultiplexing, low-quality base reads were trimmed with Trimmomatic[53] using the following parameters: LEADING: 15, TRAILING: 15, SLIDINGWINDOW: 4:15, MINLEN: 16. Trimmed reads were then aligned to the mm10 mouse genome using Bowtie2. HTSeq was used to map aligned reads to genes and to generate a gene count matrix. Normalized counts and differential expression analysis were performed using the DESeq2 R package. We performed gene set enrichment analysis as previously described[54] using signatures from the Hallmark database, the MSigDB collection and from our prior analysis of exhausted CD8$^+$ T cells from the spleens of LCMV clone 13 infected mice or from B16-OVA tumors[4].

Single-cell RNA-seq library preparation and analysis. Cotransferred control or *Ptpn2*-deleted P14 CD8$^+$ T cells were sorted from spleens of day 30 LCMV clone 13 infected, CD4-depleted mice on the basis of the markers CD8β, CD45.1, CD45.2, Vex and fixable live/dead. Cells were counted and loaded onto the Chromium Controller (10× Genomics) for a target recovery of 5,000 single cells. Samples were processed per the manufacturer's protocol and sequenced on an Illumina NextSeq500 sequencer using a 75-base-pair kit with paired-end reads. The Cell Ranger analysis pipeline v.1.2 was used for sample demultiplexing,

barcode processing, alignment, filtering, unique molecular identifier counting and aggregation of sequencing runs. The R Seurat package[55] was used for downstream analyses.

For each cell, two quality control metrics were calculated: (1) the total number of genes detected; and (2) the proportion of unique molecular identifiers contributed by mitochondrially encoded transcripts. Cells were excluded from downstream analysis if fewer than 200 or greater than 2,500 genes were detected and if mitochondrially encoded transcripts constituted greater than 5% of the total library, yielding an expression matrix of 7,027 cells by 13,133 genes. Each gene expression measurement was normalized by total expression within the corresponding cell and multiplied by a scaling factor of 10,000.
Mean and dispersion values were calculated for each gene across all cells; 1,829 genes were classified as highly variable. Highly variable genes were used for principal components analysis. Principal components were determined to be significant ($P < 0.001$) using the jackstraw method and tSNE was performed on these key principal components (1–17) using default parameters for 1,000 iterations for visualization in two dimensions. Unsupervised clustering was performed using a shared nearest neighbor modularity optimization-based algorithm[56]. Single-cell signature scoring using FastProject[57] was performed with the Hallmark database from MSigDB and using signatures of the subpopulations derived from our prior analysis of exhausted $CD8^+$ splenocytes from LCMV clone 13 infected mice[4]. Differential gene expression and signature enrichment analysis was performed using a two-sided Wilcoxon rank sum test. To determine the relative proportion of *Ptpn2*-deleted cells within each cluster, a two-sided binomial test was performed against the proportion of *Ptpn2*-deleted cells within the total dataset.

Statistical analysis. Statistical analyses were performed using GraphPad Prism 7 software or R 3.3.1. Data were considered statistically significant with P values <0.05 by a two-sided paired Student's t-test for comparing two groups in cotransfer experiments, two-sided unpaired Student's t-test for comparing two groups, one-way analysis of variance (ANOVA) for single comparisons with groups greater than two, two-way ANOVA for repeated measures comparisons or for multiple comparisons within groups, and a two-sided log-rank Mantel–Cox test for survival analysis. For GSEA of RNA-seq data a two-sided Kolmogorov–Smirnov test was used. For analysis of single-cell RNA-seq data, a two-sided Wilcoxon rank sum test was used for signature enrichments and a two-sided binomial test was used to determine proportional differences of control or *Ptpn2*-deleted cells in the clusters. For ATAC-seq analysis a hypergeometric test was used. Please see the Reporting Summary for additional details.

Reporting Summary. Further information on research design is available in the Nature Research Reporting Summary linked to this article.

Data availability

The data and materials that support the findings of this study are available from the corresponding author upon reasonable request. All sequencing data from this study has been deposited in the National Center for Biotechnology Information Gene Expression Omnibus and are accessible through the Gene Expression Omnibus Series accession code GSE134413.

References

47. Platt, R. J. et al. CRISPR-Cas9 knockin mice for genome editing and cancer modeling. *Cell* **159**, 440–455 (2014).
48. Doench, J. G. et al. Optimized sgRNA design to maximize activity and minimize off-target effects of CRISPR-Cas9. *Nat. Biotechnol.* **34**, 184–191 (2016).
49. Juneja, V. R. et al. PD-L1 on tumor cells is sufficient for immune evasion in immunogenic tumors and inhibits CD8 T cell cytotoxicity. *J. Exp. Med.* **214**, 895–904 (2017).
50. Corces, M. R. et al. Lineage-specific and single-cell chromatin accessibility charts human hematopoiesis and leukemia evolution. *Nat. Genet.* **48**, 1193–1203 (2016).
51. Buenrostro, J. D., Giresi, P. G., Zaba, L. C., Chang, H. Y. & Greenleaf, W. J. Transposition of native chromatin for fast and sensitive epigenomic profiling of open chromatin, DNA-binding proteins and nucleosome position. *Nat. Methods* **10**, 1213–1218 (2013).
52. Trombetta, J. J. et al. Preparation of single-cell RNA-seq libraries for next generation sequencing. *Curr. Protoc. Mol. Biol.* **107**, 4 22 21–17 (2014).
53. Bolger, A. M., Lohse, M. & Usadel, B. Trimmomatic: a flexible trimmer for Illumina sequence data. *Bioinformatics* **30**, 2114–2120 (2014).
54. Subramanian, A. et al. Gene set enrichment analysis: a knowledge-based approach for interpreting genome-wide expression profiles. *Proc. Natl Acad. Sci. USA* **102**, 15545–15550 (2005).
55. Satija, R., Farrell, J. A., Gennert, D., Schier, A. F. & Regev, A. Spatial reconstruction of single-cell gene expression data. *Nat. Biotechnol.* **33**, 495–502 (2015).
56. Waltman, L. & van Eck, N. J. A smart local moving algorithm for large-scale modularity-based community detection. *Eur. Phys. J. B* **86**, 471 (2013).
57. De Tomaso, D. & Yosef, N. FastProject: a tool for low-dimensional analysis of single-cell RNA-Seq data. *BMC Bioinform.* **17**, 315 (2016).

Corresponding author(s): Arlene H. Sharpe
W. Nicholas Haining

Last updated by author(s): 07/17/2019

Reporting Summary

Nature Research wishes to improve the reproducibility of the work that we publish. This form provides structure for consistency and transparency in reporting. For further information on Nature Research policies, see Authors & Referees and the Editorial Policy Checklist.

Statistics

For all statistical analyses, confirm that the following items are present in the figure legend, table legend, main text, or Methods section.

n/a	Confirmed
☐	☒ The exact sample size (*n*) for each experimental group/condition, given as a discrete number and unit of measurement
☐	☒ A statement on whether measurements were taken from distinct samples or whether the same sample was measured repeatedly
☐	☒ The statistical test(s) used AND whether they are one- or two-sided *Only common tests should be described solely by name; describe more complex techniques in the Methods section.*
☒	☐ A description of all covariates tested
☐	☒ A description of any assumptions or corrections, such as tests of normality and adjustment for multiple comparisons
☐	☒ A full description of the statistical parameters including central tendency (e.g. means) or other basic estimates (e.g. regression coefficient) AND variation (e.g. standard deviation) or associated estimates of uncertainty (e.g. confidence intervals)
☐	☒ For null hypothesis testing, the test statistic (e.g. *F*, *t*, *r*) with confidence intervals, effect sizes, degrees of freedom and *P* value noted *Give P values as exact values whenever suitable.*
☒	☐ For Bayesian analysis, information on the choice of priors and Markov chain Monte Carlo settings
☒	☐ For hierarchical and complex designs, identification of the appropriate level for tests and full reporting of outcomes
☒	☐ Estimates of effect sizes (e.g. Cohen's *d*, Pearson's *r*), indicating how they were calculated

Our web collection on statistics for biologists contains articles on many of the points above.

Software and code

Policy information about availability of computer code

Data collection	Flow analysis was performed using FACSDIVA version 8.0.1 (BD Pharmingen). Flow sorting was performed using FACSDIVA versions 6.1.3 or 8.0.2 (BD Pharmingen). Sequencing data was collected on a NextSeq500 (Illumina) or ABI3730xl DNA analyzer (Thermo Fisher Scientific).
Data analysis	All flow data was analyzed using FlowJo version 10.4.2. All statistical tests were run using Graphpad Prism 7 or R 3.3.1. Sanger sequencing for the TIDE assay was analyzed on the online TIDE webtool. ATAC-seq data was processed/analyzed using Trimmomatic 0.33, Bowtie 2.2.4, MACS 2.1.1, Samtools 1.3, DESeq2, and Genomics Viewer 2.3.77. Bulk RNA-seq data was processed/analyzed using Trimmomatic 0.36, Bowtie 2, HTSeq, and DESeq2. Single-cell RNA-seq was processed/analyzed using the Cell Ranger analysis pipeline 1.2, the R Seurat package 2.4, and FastProject 1.1.4.

For manuscripts utilizing custom algorithms or software that are central to the research but not yet described in published literature, software must be made available to editors/reviewers. We strongly encourage code deposition in a community repository (e.g. GitHub). See the Nature Research guidelines for submitting code & software for further information.

Data

Policy information about availability of data

All manuscripts must include a data availability statement. This statement should provide the following information, where applicable:

- Accession codes, unique identifiers, or web links for publicly available datasets
- A list of figures that have associated raw data
- A description of any restrictions on data availability

The data and materials that support the findings of this study are available from the corresponding author upon reasonable request. All sequencing data from this study has been deposited in the National Center for Biotechnology Information Gene Expression Omnibus (GEO) and are accessible through the GEO Series accession code GSE134413.

Field-specific reporting

Please select the one below that is the best fit for your research. If you are not sure, read the appropriate sections before making your selection.

☒ Life sciences ☐ Behavioural & social sciences ☐ Ecological, evolutionary & environmental sciences

For a reference copy of the document with all sections, see nature.com/documents/nr-reporting-summary-flat.pdf

Life sciences study design

All studies must disclose on these points even when the disclosure is negative.

Sample size	Sample size was chosen to ensure the possibility of statistical analysis and to also minimize the use of animals in accordance with animal care guidelines from the Harvard Medical School Standing Committee on Animals and the National Institutes of Health. The results from previous results were also used to determine the sample size.
Data exclusions	For single-cell RNA-seq, two quality control metrics were calculated for each cell: (1) the total number of genes detected and (2) the proportion of UMIs contributed by mitochondrially encoded transcripts. Cells were excluded from downstream analysis if fewer than 200 genes or greater than 2500 genes were detected and if mitochondrially encoded transcripts constituted greater than 5% of the total library. These were pre-determined exclusion criteria based on standard Seurat parameters to exclude cells that had poor capture of transcripts (low recovery of genes), doublets (high recovery of genes), or were dying (high percentage of mitochrondrially encoded transcripts). Data was not excluded for any other experiment.
Replication	Replicates were used in all experiments as noted in the text and figure legends. All experiments presented for which replication was attempted were successfully replicated.
Randomization	Age and sex-matched animals were used for each experiment. Animals were also co-housed when possible.
Blinding	LCMV Clone 13 infection and tumor experiments were blinded during data collection where possible (Figures 4j, 5g-5i, 6g-6h, 7b-7j and Supplementary Figures 2f, 4e-4f, 5f-5g, 7d-7m). All co-transfer experiments are inherently blinded.

Reporting for specific materials, systems and methods

We require information from authors about some types of materials, experimental systems and methods used in many studies. Here, indicate whether each material, system or method listed is relevant to your study. If you are not sure if a list item applies to your research, read the appropriate section before selecting a response.

Materials & experimental systems

n/a	Involved in the study
☐	☒ Antibodies
☐	☒ Eukaryotic cell lines
☒	☐ Palaeontology
☐	☒ Animals and other organisms
☒	☐ Human research participants
☒	☐ Clinical data

Methods

n/a	Involved in the study
☒	☐ ChIP-seq
☐	☒ Flow cytometry
☒	☐ MRI-based neuroimaging

Antibodies

Antibodies used	Antibodies and dyes were purchased from BD Biosciences (7-AAD Cat# 559925 (1:100 dilution), Slamf6 Clone 13G3 Cat# 561540 (1:100 dilution), BrdU Clone 3D4 Cat# 552598 (1:50 dilution), Ki67-PerCP-Cy5.5 Clone B56 Cat# 561284 (1:100 dilution)); Biolegend (B220 Clone RA3-6B2 Cat# 103208, 103226 (1:100 dilution), CD11b Clone M1/70 Cat# 101208, 101216 (1:100 dilution), CD127 Clone A7R34 Cat# 135014, 135024 (1:100 dilution), CD25 Clone PC61 Cat# 101904 (1:100 dilution), CD3ε Clone 17A2 Cat# 100220, 100308, 100336, 100328 (1:100 dilution), CD4 Clone RM4-5 Cat# 100516, 100531, 100543 (1:100 dilution), CD44 Clone IM7 Cat# 103008, 103028, 103030 (1:100 dilution), CD45.1 Clone A20 Cat# 110708, 110716, 110741 (1:100 dilution), CD45.2 Clone 104 Cat# 109824, 109832, 109830 (1:100 dilution), CD5 Clone 53-7.3 Cat# 100608 (1:100 dilution), CD62L Clone MEL-14 Cat# 104417 (1:100 dilution), CD8α Clone 53-6.7 Cat# 100737 (1:100 dilution), CD8β Clone YTS156.7.7 Cat# 126606, 126608, 126610, 126620, 126614 (1:100 dilution), c-Kit Clone ACK2 Cat# 135108 (1:100 dilution), CXCR5 Clone L138D7 Cat# 145509 (1:50 dilution), Gr-1 Clone RB6-8C5 Cat# 108408 (1:100 dilution), Granzyme B Clone GB11 Cat# 515403, 515406 (1:100 dilution), I-A/I-E Clone M5/114.15.2 Cat# 107614 (1:100 dilution), IFN-γ Clone XMG1.2 Cat# 505810 (1:100 dilution), IFNAR1 Clone MAR1-5A3 Cat# 127314 (1:100 dilution), Ly-6c Clone HK1.4 Cat# 128007 (1:100 dilution), PD-1 Clone 29F.1A12 Cat# 135206, 135209 (1:100 dilution), Sca-1 Clone D7 Cat# 108108, 108128 (1:100 dilution), TCR Vα2 Clone B20.1 Cat# 127814, 127806 (1:100 dilution), TCR Vβ5 Clone MR9-4 Cat# 139506 (1:100 dilution), TCR Vβ8 Clone KJ16-133.18 Cat# 118406 (1:100 dilution), TER-119 Clone TER-119 Cat# 116208 (1:100 dilution), TCF1 Clone 7F11A10 Cat# 655208 (1:100 dilution), Tim-3 Clone RMT3-23 Cat# 119703, 119723 (1:100 dilution), TNF Clone MP6-XT22 Cat# 506322 (1:100 dilution), TruStain fcX Clone 93 Cat# 101320 (1:50 dilution), Rat IgG2a κ Isotype Clone RTK2758 Cat# 400508 (1:100 dilution), Rat IgG2b κ Isotype Clone RTK4530 Cat#

400612 (1:100 dilution), Streptavidin Cat# 405225 (1:400)); Invitrogen anti-GFP (Polyclonal) Cat#A21311 (1:350 dilution); Thermo Fisher Scientific (Foxp3 Clone FJK-16s Cat# 48-5773-82 (1:50 dilution), Cell Trace Violet Proliferation Dye Cat# C34557 (1 uM), Near-IR Fixable Live/Dead Cat# L34976 (1:500 dilution)); and Cell Signaling Technology pSTAT1 Clone 58D6 Cat# 9174 (1:100 dilution).

Validation

Representative flow cytometry plots are shown in Figures 1, 2, 4, and 6 and Supplementary Figures 1, 2, 4-7. Further validation is present on the manufacturer's website for antibodies noted in the Methods section.

Eukaryotic cell lines

Policy information about cell lines

Cell line source(s)	MC38-OVA, B16-OVA, and MC38-GP33-41 cells were created in the Sharpe and Haining labs. BHK and Vero cells were a gift from E. John Wherry. 293x cells were a gift from C. Kadoch. B16.F10 and B16/GMCSF cells were gifts from G. Dranoff.
Authentication	MC38 and B16 parental cells were validated through whole exome sequencing. MC38-OVA and B16-OVA cells were validated based on selection in puromycin. MC38 GP33-41 cells were validated by flow cytometry based on expression of the selectable marker GFP. B16/GMCSF cells were validated by ELISA.
Mycoplasma contamination	All cell lines were confirmed mycoplasma negative.
Commonly misidentified lines (See ICLAC register)	293x (clone of HEK). These cells were used in the production of lentivirus which was validated by titering.

Animals and other organisms

Policy information about studies involving animals; ARRIVE guidelines recommended for reporting animal research

Laboratory animals	Female/male C57BL/6J mice were purchased from The Jackson Laboratory and used at age 7-10 weeks. C57BL/6-Tg(Zp3-cre)1Gwh/J, C57BL/6-Tg(TcraTcrb)1100Mjb/J, and B6.SJL-Ptprca Pepcb/BoyJ mice were purchased from The Jackson Laboratory and bred to B6J.129(B6N)-Gt(ROSA) 26Sortm1(CAG-cas9*,-EGFP)Fezh/J mice (a gift from F. Zhang). B6.Cg-Tcratm1Mom Tg(TcrLCMV)327Sdz mice were purchased from Taconic, backcrossed >10 generations to C57BL/6J from The Jackson Laboratory, and then bred to B6J.129(B6N)-Gt(ROSA) 26Sortm1(CAG-cas9*,-EGFP)Fezh/J mice. These strains (both female and male) were used at 8-16 weeks of age for donor bone marrow to create bone marrow chimeras. Resulting bone marrow chimeras were used at 14-20 weeks of age. Within a given experiment all stages of the experiment were sex-matched (bone marrow donor, bone marrow recipient, and transferred cell recipient).
Wild animals	The study did not involve wild animals.
Field-collected samples	The study did not involve field-collected samples.
Ethics oversight	HMA Standing Committee on Animals

Note that full information on the approval of the study protocol must also be provided in the manuscript.

Flow Cytometry

Plots

Confirm that:

☒ The axis labels state the marker and fluorochrome used (e.g. CD4-FITC).

☒ The axis scales are clearly visible. Include numbers along axes only for bottom left plot of group (a 'group' is an analysis of identical markers).

☒ All plots are contour plots with outliers or pseudocolor plots.

☒ A numerical value for number of cells or percentage (with statistics) is provided.

Methodology

Sample preparation	Bones were excised, mechanically crushed, filtered to single-cell suspension, ACK lysed, c-Kit MACS purified, and sorted. Spleen and lymph nodes were dissected from mice, mechanically minced, and filtered to single-cell suspension. RBC lysis was performed on spleen samples that were not MACS purified. Blood samples were isolated by retro-orbital bleed and enriched for lymphocytes on a Histopaque-1083 gradient. Blood samples isolated via the tail vein were ACK lysed. Livers were excised, mechanically minced, filtered to single-cell suspension, and enriched for lymphocytes on a Percoll gradient. Tumors were dissected from the surrounding fascia, mechanically minced, treated with collagenase for 10 minutes at 37°C, and filtered to single-cell suspension. Tumor-infiltrating leukocytes were enriched using an Optiprep gradient. When necessary, cells were sorted on a FACS Aria II (BD Biosciences) to obtain greater than 95% purity.
Instrument	BD LSR II or BD Symphony A5 were used to collect data for analysis. BD FACSAria II was used for cell sorting.

Software	All flow data was collected using FACSDIVA versions 6.1.3, 8.0.1, or 8.0.2 (BD Pharmingen) and analyzed using FlowJo version 10.4.2.
Cell population abundance	All sorts had a purity > 95%, checked by post-sort re-sampling.
Gating strategy	Gating strategy summarized in Figure 2 and Supplementary Figures 1 and 6, with gates drawn based on single-stain and full-minus-one (FMO) controls.

☒ Tick this box to confirm that a figure exemplifying the gating strategy is provided in the Supplementary Information.